의학박사 학위논문

Analysis of Tumor Immune Microenvironment of a Novel Orthotopic Anaplastic Thyroid Cancer Model Developed in C57BL/6 Mice

C57BL/6 마우스에서의 정위이식 역형성 갑상선암 모델 구축 및 종양 면역 미세환경 분석

2023년 8월

서울대학교 대학원

의학과 외과학 전공

허 진

C57BL/6 마우스에서의 정위이식 역형성 갑상선암 모델 구축 및 종양 면역 미세환경 분석

지도교수 이 규 언

이 논문을 의학박사 학위논문으로 제출함
2023년 4월

서울대학교 대학원
의학과 외과학 전공
허 진

허진의 의학박사 학위논문을 인준함
2023년 8월

위 원 장 _____ (인)
부위원장 _____ (인)
위 원 _____ (인)
위 원 _____ (인)
위 원 _____ (인)

Abstract

Zhen Xu
Department of Surgery
The Graduate School
Seoul National University

Background: Securing a well-established mouse model is important in identifying and validating new therapeutic targets for immuno-oncology. The C57BL/6 mouse is one of the most fully characterised immune system of any animal and provides powerful platform for immuno-oncology discovery. An orthotopic tumor model has been established using TBP3743 (murine anaplastic thyroid cancer [ATC]) cells in B6129SF1 hybrid mice, this model has limited data on tumor immunology than C57BL/6 inbred mice. This study aimed to establish a novel orthotopic ATC model in C57BL/6 mice and characterize the tumor microenvironment focusing immunity in the model.

Methods: Adapted TBP3743 cells were generated via in vivo serial passaging in C57BL/6 mice. Subsequently, the following orthotopic tumor models were established via intrathyroidal injection: B6129SF1 mice injected with original TBP3743 cells (original/129), B6129SF1 mice injected with adapted cells (adapted/129), and C57BL/6 mice injected with adapted cells (adapted/B6).

Results: The adapted TBP3743 cells de-differentiated but exhibited cell morphology, viability, and migration/invasion potential comparable with those of original cells in vitro. The adapted/129 contained a higher Ki-67$^+$ cell fraction than the original/129. RNA sequencing data of orthotopic tumors revealed enhanced oncogenic properties in the adapted/129 compared with those in the original/129. In contrast, the orthotopic tumors grown in the adapted/B6 were smaller, with a lower Ki-67$^+$ cell fraction than those in the adapted/129. However, the oncogenic properties of the tumors within the adapted/B6 and adapted/129 were similar. Immune-related pathways were enriched in the adapted/B6 compared with those in the adapted/129. Flow cytometric analysis of the orthotopic tumors revealed higher cytotoxic CD8$^+$ T cell and monocytic-myeloid-derived suppressor cell fractions in the adapted/B6 compared with the adapted/129. The estimated CD8$^+$ and CD4$^+$ cell fractions in the adapted/B6 were similar to those in human ATCs but negligible in the original/B6.

Conclusions: A novel orthotopic tumor model of ATC was established in C57BL/6 mice. Compared with the original B6129SF1 murine model, the novel model exhibited more aggressive tumor cell behaviours and strong immune responses. Expect that this novel model contributes to the understanding tumor

microenvironment and provides the platform for drug development.

Keyword: Anaplastic thyroid cancer, syngenic, tumor microenvironment, immunotherapy

Student Number: 2017-36136

CONTENTS

LIST OF FIGURES

LIST OF TABLES

Introduction

Anaplastic thyroid carcinoma (ATC) is a highly aggressive malignant tumor accounting for 1–2% of all thyroid cancers.(1–5) Upon initial presentation, most patients exhibit extensive local invasion or distant metastatic lesions (stage IVA–IVC).(2) Thus, the associated prognosis is poor, with a median overall survival of 5–12 months.(2, 4, 6)

Tremendous research efforts have sought to characterize the genetic and molecular pathogenesis of ATC,(4, 7–9) leading to the development of novel targeted therapies. For instance, the $BRAF^{V600E}$ mutation is frequently found in ATCs (20–50% of the cases).(7, 8, 10) The combination therapy of BRAF and MEK inhibitors has demonstrated therapeutic efficacy in $BRAF^{V600E}$–mutated ATCs,(11) leading to its approval in 2018 by the United States Food and Drug Administration. However, progression–free and median overall survival remain relatively low (6.7 and 14.5 months, respectively) even after the combination therapy.(12)

One of requirements for the development of anti–cancer drugs is the establishment of a mouse model that replicates the histology and microenvironment of human tumors.(13) The cultivated cell–line derived xenograft model (CDXM) is currently the most widely used model for drug screening and development.(14) Although the

CDXM exhibits rapid tumor development and excellent experimental reproducibility, it is unsuitable for investigating tumor microenvironments as it is established in immune-compromised mice. Meanwhile, the genetically engineered model (GEM) has been successfully applied to replicate and analyse tumor microenvironments. However, tumor formation requires a longer period in the GEM than in the xenograft model, and the rate of tumor formation varies among mice.(15-17) Thus, by combining the advantages of the CDXM and GEM, a model for transplanting murine tumor cells from the GEM back into mice has been developed. The TBP3743 murine ATC cell line generated from mice with a thyroid-specific *Braf*^{V600E} mutation and *Trp53* and *Pten* deletion(18, 19) exhibits rapid and consistent tumor growth following orthotopic injection in B6129SF1 hybrid mice.(19) Although this model has been tried to explore the tumor microenvironment and assess the anti-tumor efficacy of immune checkpoint inhibitors,(20) B6129SF1 hybrid mice have little cumulative data regarding tumor biology and drug development compared to inbred C57BL/6 mice.(21)

In this study, *in vivo* adaptation of TBP3743 cells within inbred C57BL/6 mice was performed, leading to the establishment of an orthotopic model of ATC. The differentiation status, oncogenic

molecular features, and immune signatures of tumors derived from the original and adapted TBP3743 cells were characterized. The findings of this study provide insights into a suitable preclinical mouse model for investigating the ATC tumor microenvironment and developing anti-cancer drugs for immunotherapy.

Methods

Maintenance of tumor cells *in vitro*

The original TBP3743 cell line,(19) generated from B6129SF1 mice with thyroid-specific *Braf*^{V600E} and thyroid-specific *Trp53* and *Pten* deletion, was kindly gifted from Dr. Sareh Parangi (Department of Surgery, Massachusetts General Hospital, Harvard Medical School, Boston, MA, USA). These cells were maintained in RPMI-1640 media supplemented with 10% fetal bovine serum (FBS; WELGENE, Seoul, Korea), 2mM GlutaMAX^{TM} (Gibco, New York, NY, USA), and 100U/mL penicillin-streptomycin (Gibco).

Generation of adapted TBP3743 cells in C57BL/6 mice

Six-week-old female C57BL/6 and B6129SF1 mice were purchased from Orient Bio Inc. (Seongnam, Korea) and the Jackson Laboratory (Bar Harbor, ME, USA), respectively. Adapted TBP3743 cells were generated by subcutaneously injecting C57BL/6 mice (n = 5) with a mixture of 1×10^7 original TBP3743 cells and Matrigel (BD Biosciences, Franklin Lakes, NJ). Two-dimensional tumor size was measured twice per week, and the tumor volume was calculated using Eq.(1): Volume = ½ × a × b^2,

where a is the longest diameter and b is the perpendicular diameter.(22) First, the mice were euthanized and the largest tumor was selected, surgically removed, minced, and incubated with phosphate-buffered saline (PBS) containing 2mg/mL collagenase type 1 on a shaker at 37℃ for 3h. The cells were then maintained in RPMI-1640 media supplemented with 10% FBS. Expanded tumor cells were re-implanted in new C57BL/6 mice (n = 5) in the same manner as described above.

Establishment of the murine orthotopic tumor model of ATC

The orthotopic tumor model was established by intrathyroidal injection of tumor cells. For intrathyroidal injection, 1×10^5 tumor cells in 10μL of PBS were injected into the left thyroid gland of mice using a Hamilton syringe with a 30G needle.

Six-week-old female C57BL/6 or B6129SF1 mice underwent intrathyroidal injection of 130 the original or adapted TBP3743 cells. The original cells were injected into the B6129SF1 mice (original/129 group). Adapted cells after 3rd and 6th adaptation passage were injected into the B6129SF1 mice (adapted/129 group) or C57BL/6 (adapted/B6 group and SC6/B6 group,

respectively). To evaluate the effect of tumor–host immune interactions in tumor growth, injected the original and adapted cells into athymic mice (Orient Bio, Inc., Seongnam, Korea). Tumor size and volume were measured 9 days after tumor cell injection.

Evaluation of the *in vivo* anti–tumor response to BRAF inhibitor in mice injected with adapted TBP3743 cells

To evaluate the anti–tumor response to a BRAF inhibitor, labelled adapted TBP3743 cells with luciferase protein before generating the orthotopic thyroid cancer model. Note that the detailed luciferase–labelling method is provided in the supplementary method. Beginning three days after tumor cell injection, mice were intraperitoneally injected daily with 10mg/kg of PLX–4032 (Selleckchem, Houston, TX, USA; n = 8) or saline (untreated group; n = 8). To obtain *in vivo* bioluminescence imaging, mice were intraperitoneally injected with 100μL (3mg/mL PBS) of D–Luciferin (Perkin Elmer, Wellesley, MA). Bioluminescence imaging (IVIS spectrum, Perkin Elmer) was performed two weeks after tumor cell injection.

Evaluation of the *in vivo* anti-tumor response to anti-PD-L1 antibody in mice injected with adapted TBP3743 cells

To evaluate the anti-tumor response to anti-PD-L1 antibody, intraperitoneally injected daily with 0.2 mg/kg of anti-PD-L1 antibody (kindly gifted from Pf. Dae Hee Kim,_Kangwon National University, Gangwon-do, Republic of Korea) or Ig G controls from 5 days after tumor cell injection. Tumor size and volume were measured 10 days after tumor cell injection.

Immunohistochemical staining

The harvested tumors were fixed in 4% paraformaldehyde and embedded in paraffin. Immunohistochemistry (IHC) staining was performed with the following primary antibodies: anti-CD3 (1:100, ab5690, Abcam, Cambridge, UK), anti-CD4 (1:100, ab183685, Abcam), anti-CD8 (1:100, ab209775, Abcam), F4/80 (1:50, 14-4801-81, Invitrogen, San Diego, CA, USA), anti-CD163 (1:200, ab182422, Abcam), and anti-Ki67 (1:200, MA5-14520, Invitrogen).

Evaluation of the *in vivo* anti-tumor response to

combination therapy in mice injected with adapted TBP3743 cells

Following orthotopic transplantation of six-week-old female C57BL/6 mice, they were divided into five groups (n = 7, each group, Control(C); BRAF inhibitor(B); BRAF inhibitor + anti-CD47(B+C); BRAF inhibitor + anti-PD-L1(B+P); BRAF inhibitor + anti-CD47 + anti-PD-L1(B+C+P)). Beginning three days after tumor cell injection, mice were subjected to intraperitoneal injections of either 10mg/kg of PLX-4032 (daily), 15mg/kg of anti-CD47 (once every two days), or 15mg/kg of anti-PD-L1 (once every two day). Mice underwent euthanasia on the day10 after drug administration to observe changes in tumor size.

The experiment was repeated for survival curve analysis. Mice was continually monitored until the humane endpoint rather than timed sacrificed.

Cell viability assay

To compare the viability of original and adapted TBP3743 cells, 8×10^3 cells/mL were seeded into a 96-well tissue culture plate with 100 μL of media. Subsequently, 10 μL of the CCK-8 solution (Dojindo, Kumamoto, Japan) was added to each well after 12, 36,

and 60 h. The cells were incubated for an additional 2 h, and the absorbance was measured at 450 nm with a microplate reader (SpectraMax 190; Molecular Devices, San Jose, CA, USA).

To assess the drug response to the BRAF inhibitor, the original and adapted TBP3743 cells (1×10^3/well) were seeded in 384-well plates and treated with PLX-4032 (0.05, 0.15, 0.46, 1.37, 4.12, 12.35, 37.03, 111.11, 333.33, or 1000μM). Cell viability was evaluated using a CellTiter-Glo Luminescent Cell Viability Assay (Promega) after 72h of PLX-4032 treatment.

Real-time PCR assay

Total RNA was extracted using TRIzol reagent (Invitrogen) from *in vitro* maintained tumor cells or *in vivo* orthotopic tumors, and cDNA was synthesized using the M-MLV Reverse Transcriptase kit (Invitrogen). The real-time PCR was performed with the StepOne Plus real-time PCR system (Applied Biosystems) and TB green Premix (Takara Bio Inc., Otsu, Japan). The assay was performed according to the manufacturer's protocol. Results were presented as the average of three independent experiments. Detailed primer sequences are listed in supplementary data.

Cell migration assay

Cell migration was assessed using the Transwell system (Corning, NY, USA). Briefly, polycarbonate membranes with 8μm pores were coated with 0.2% gelatin solution for 1h and dried overnight. Cells were added to the upper chamber and placed into a 24-well plate. The lower chamber was filled with 650μL of serum-free media. After 12h, non-migrating cells were swabbed with a cotton-tipped applicator. Migrating cells to lower chamber were fixed in methanol for 30min, and stained with 1% crystal violet for 30min. The results were quantified with ImageJ.

3D invasion assay

A 3D invasion assay was performed with the original and adapted TBP3743 cells using a Cultrex 3D Spheroid Cell Invasion Assay (Trevigen, Inc., Gaithersburg, MD, USA). Briefly, 2×10^3 cells were dispensed in 50μL of Spheroid Formation Extracellular Matrix (ECM) per well and incubated at 37℃ for 72h. After three days, 50μL of the Invasion Matrix was added to each well and incubated at 37℃ for seven days. Cell invasion was observed microscopically using the 4×objective, and spheroid images were analysed by ImageJ.

Flow cytometry

Tumors were minced and incubated with Hanks' Balanced Salt solution (HBSS) containing 2mg/mL collagenase type 1 on a shaker at 37℃ for 3h. Cells were washed and suspended in PBS supplemented with 2% FBS, followed by staining with fluorochrome-conjugated antibodies: anti-CD45 (1:250, 103138, BioLegend, San Diego, CA, USA), anti-CD3 (1:60, 35-0031-82, Invitrogen), anti-CD4 (1:60, 100422, BioLegend), anti-CD8 (1:60, 100714, BioLegend), anti-CD25 (1:10, MA5-17818, Invitrogen), anti-FoxP3 (1:10, 17-5773-82, Invitrogen), anti-CD11b (1:50, 101206, BioLegend), anti-Ly6C (1:50, 128026, BioLegend), anti-Ly6G (1:100, 560599, BD Biosciences, Franklin Lakes, NJ, USA), anti-F4/80 (1:50, 12-4801-82, Invitrogen), anti-CD80 (1:50, 562504, BD Biosciences), and anti-CD206 (1:50, 46-2061-82, Invitrogen), anti-MHC Class 1 (1:50, ab95572, Abcam), and anti-NK1.1 (1:50, 61-5941-82, Invitrogen). Multicolour flow cytometry was performed using The MACSQuant® Analyzer 16 (Miltenyi Biotec B.V. & Co. KG, Bergisch Gladbach, Germany) and analysed with FlowJo software (BD Biosciences, OR, USA).

Bulk RNA sequencing and data analysis

RNA was isolated from three tumor tissues in the original/129, adapted/129, and adapted/B6 groups. Total RNA was used to construct cDNA libraries with the TrueSeq RNA library kit (Illumina, San Diego, CA, USA) according to the manufacturer's instructions. Next, sequencing was performed using an Illumina HiSeq2000 (Illumina) platform with ~100nt paired-end reads. The quality of raw sequence data was assessed using FastQC (FastQC 0.11.3). Sequenced reads were aligned to the mm10 mouse genome assembly (GRCm38) reference genome with HISAT2 aligner (HISAT2 2.2.1). Raw read counts were used to analyse the differentially expressed genes (DEGs) among the groups by applying the Cuffdiff workflow (Cuffdiff 2.2.1). DEGs were defined as genes with a false discovery rate (FDR) < 0.05 and an absolute log2 fold change >1.

Curated gene sets were derived from the Kyoto Encyclopedia of Genes and Genomes (KEGG) pathway database and the Broad Institute Molecular Signatures Database. Over-representation analysis with the DEGs was performed using the DAVID functional annotation tool, and enriched gene sets were those with an FDR < 0.05. Single sample gene set enrichment analysis (ssGSEA) was performed with R package gene set variation analysis.

In the network analysis, nodes represented enriched gene sets that were significantly over-represented by DEGs, while edges represented gene expression profiles that were significantly correlated (similarity > 0.5) across samples/gene sets. Interpretation and plotting of the network were performed with R package igraph.

Immune cell proportions were analysed by CIBERSORT using the LM22 gene signature. Gene expression data of tumors from original/129, adapted/129, or adapted/B6, as well as human ATCs from the previously published data(8) were normalized as fragments per kilobase of transcript per million (FPKM) by Cuffnorm and uploaded to the CIBERSORT web portal (https://cibersort.stanford.edu/). Twenty-two human hematopoietic cell proportions per sample were provided.

Statistical analysis

Statistical analyses were performed using GraphPad PRISM version 8.0.0 (GraphPad Software, San Diego, CA, USA). Data were presented as mean ± standard deviation. The independent *t*-test, paired *t*-test, or Mann-Whitney U-test ($n < 10$) was used to compare continuous variables. Statistical significance was defined as two-sided *P*-values < 0.05. Statistical analyses and plotting for

bulk RNA sequencing were performed using R Statistical Software (version 4.0.3).

Results

Establishment of the adapted TBP3743 cell line via *in vivo* passaging to the C57BL/6 mice

To generate the adapted TBP3743 cells in C57BL/6 mice, six rounds of *in vivo* serial passaging were performed (**Fig. 1A**). Cells harvested from round−1, −3, and −6 tumors were designated as SC1, SC3, and SC6 cells, respectively, and injected into another C57BL/6 mouse for the subsequent round. Tumors after rounds 3 were stably established three weeks after the injection (**Table 1**). SC3 and SC6 exhibited comparable tumor growth *in vivo* (**Fig. 1B**). The gross morphology of the original cells was similar to those of SC1, SC3, and SC6 cells (**Fig. 1C**). The $Braf^{V600E}$ mutation was identified in all SC1−4 cells (**Fig. 2**). Then compared the expression of genes associated with thyroid differentiation. The mRNA expressions of *Tshr*, *Pax8*, *Nis*, and *Ttf1* were significantly downregulated in SC3 and SC6 cells compared with the original TBP3743 cells, but comparable between SC3 and SC6 (**Fig. 1D**). Consistently, protein expression of PAX8 was completely lost in SC3 and SC6, and that of TTF1 was lower, but still preserved in SC3 and SC6 compared with the original TBP3743 cells. TSHR protein expression was negligible in the original cell, SC3, and SC6

(**Fig. 3**). In addition, the expression of *Igf2bp1*, which has recently been identified as a marker for ATC (23), was observed to be significantly downregulated gradually from the original state to SC3 and further to SC6 (**Fig. 1D**). In summary, the SC3 and SC6 cells were de-differentiated clones compared with the original cells. *In vivo* tumorigenic capacities between SC3 and SC6 in C57BL/6 mice were similar. *In vitro* cell morphology and the expressions of thyroid differentiation genes were all comparable between SC3 and SC6. Both SC3 and SC6 maintained the molecular characteristics of ATC. Thus, designated SC3 as the adapted TBP3743 cells for further use.

Next, *in vitro* characteristics were investigated between the original and adapted TBP3743 cells. Cell viability was similar between two cell types **(Fig. 1E)**. The migration **(Fig. 1F and Fig. 4)** and invasion **(Fig. 1G)** capacity of these two cells were also comparable. Consistent with a previous report (19), loss of E-cadherin was observed in both cells. The abundances of N-cadherin and vimentin were similar (**Fig. 5A**). Regarding oncogenic signaling, the phosphorylation of AKT was significantly increased in the adapted TBP3743 cells compared to the original cells (**Fig. 5B**). Additionally, ERK phosphorylation was higher in the adapted TBP3743 cells compared to the original cells, but the difference did

not reach statistical significance (**Fig. 5B**). Collectively, cell viability, migration, and invasion capacity were similar between the original and adapted cells, while the PI3K–AKT pathway showed a modest increase in the adapted TBP3743 cells compared with the original cells.

Figure 1

A.

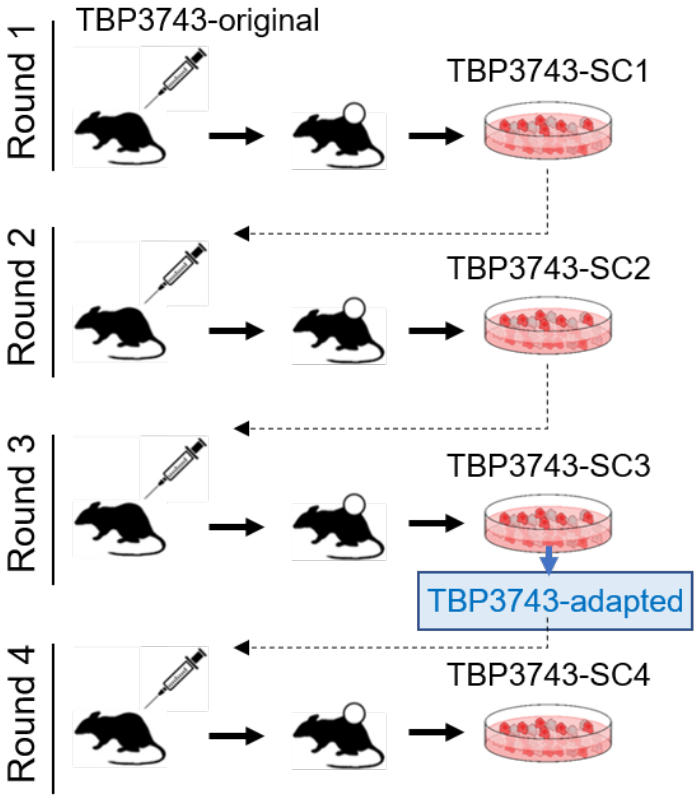
TBP3743-original
Round 1
TBP3743-SC1
Round 2
TBP3743-SC2
Round 3
TBP3743-SC3
TBP3743-adapted
Round 4
TBP3743-SC4

B.

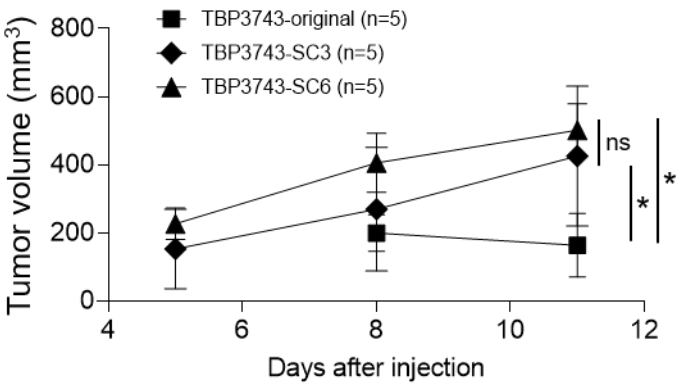
TBP3743-original (n=5)
TBP3743-SC3 (n=5)
TBP3743-SC6 (n=5)
Tumor volume (mm3)
800
600
400
200
0
4
6
8
10
12
Days after injection
ns
*
*

C.

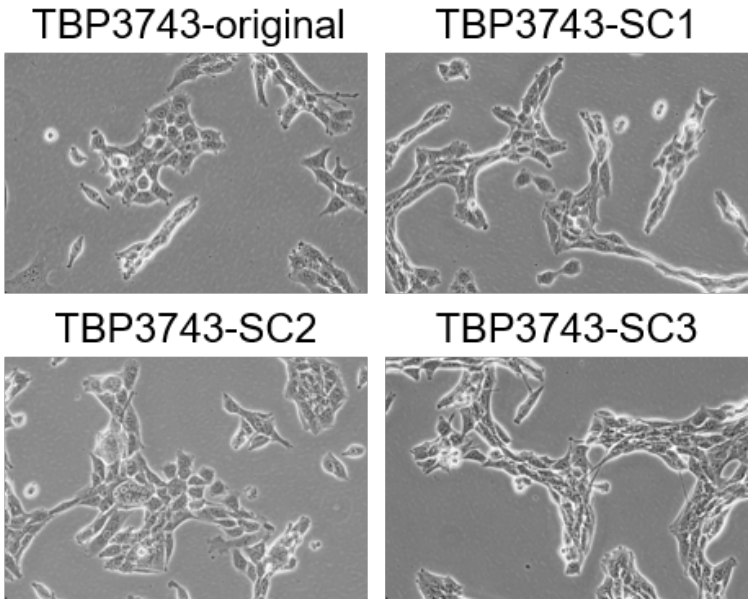
TBP3743-original
TBP3743-SC1
TBP3743-SC2
TBP3743-SC3

D.

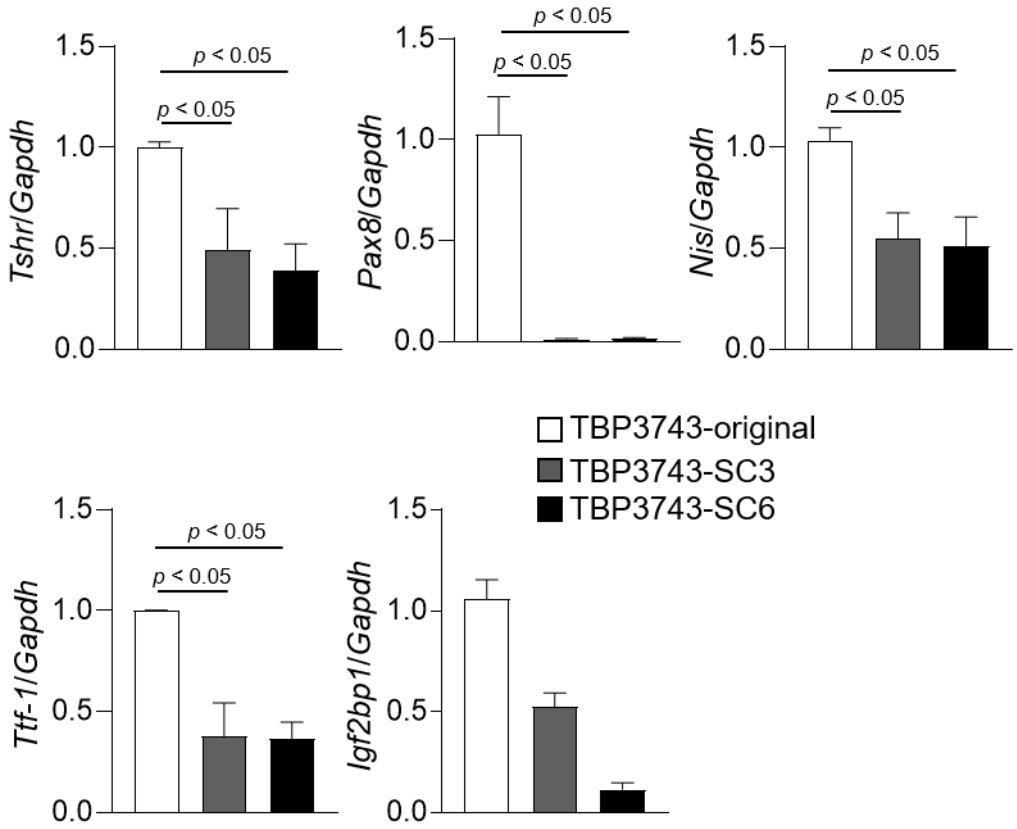
Tshr/Gapdh
Pax8/Gapdh
Nis/Gapdh
Ttf-1/Gapdh
Igf2bp1/Gapdh
p < 0.05
1.5
1.0
0.5
0.0
TBP3743-original
TBP3743-SC3
TBP3743-SC6

E.

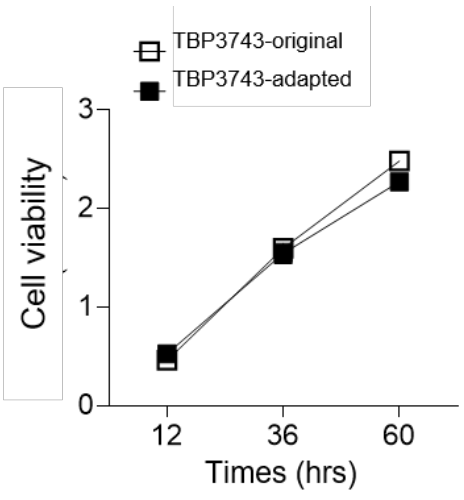
TBP3743-original
TBP3743-adapted
Cell viability
3
2
1
0
12
36
60
Times (hrs)

F. G.

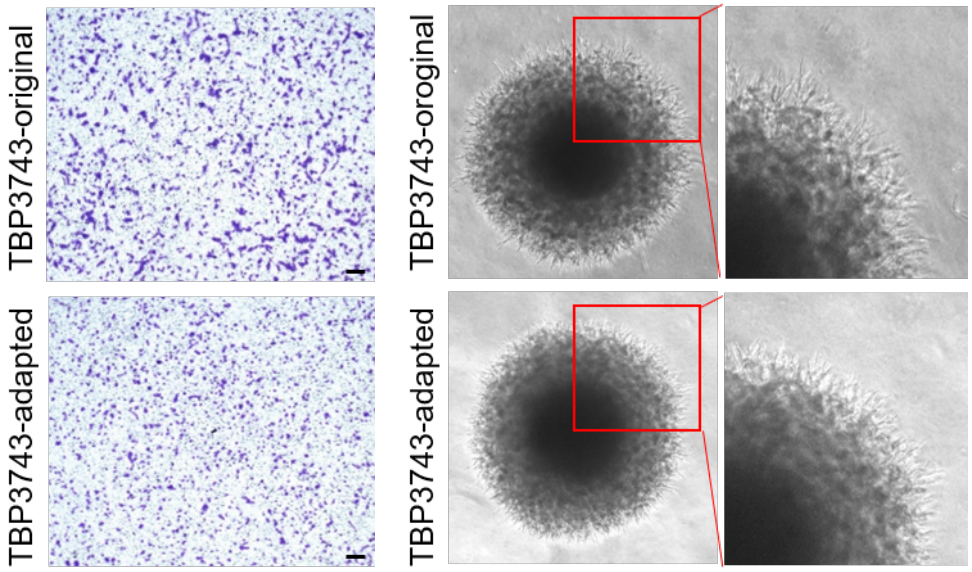

Figure 1. In vivo passaging of TBP3743 cells.

TBP3743 cells were subcutaneously injected into C57BL/6 mice and tumor growth were observed for 21 days in 1st and 2nd round, and 10-15 days in 3rd, 4th 5th, and 6th round of in vivo passaging. At each round, the two largest tumors were harvested, primary single cell culture were performed, and established cells were used for the next round of in vivo passaging. (A) Scheme for TBP3743 adaptation into C57BL/6 mice. (B) Tumor growth curves of the original, 3rd and 6th round from day 5 to 11. (C) The morphology of TBP3743 original or subclones cells (scale bars: 200 μm). (D) Thyroid differentiation related genes were analyzed by real-time

RT-PCR. To characterize TBP3743-original or -adapted cells, (E) proliferation were measured by the CCK-8 assay at the indicated time, (F) cell migration assay were performed using Transwell system (scale bars: 50 μm), (G) cell invasion ability were measured by spheroid culture system. SC, subclone.

Figure 2

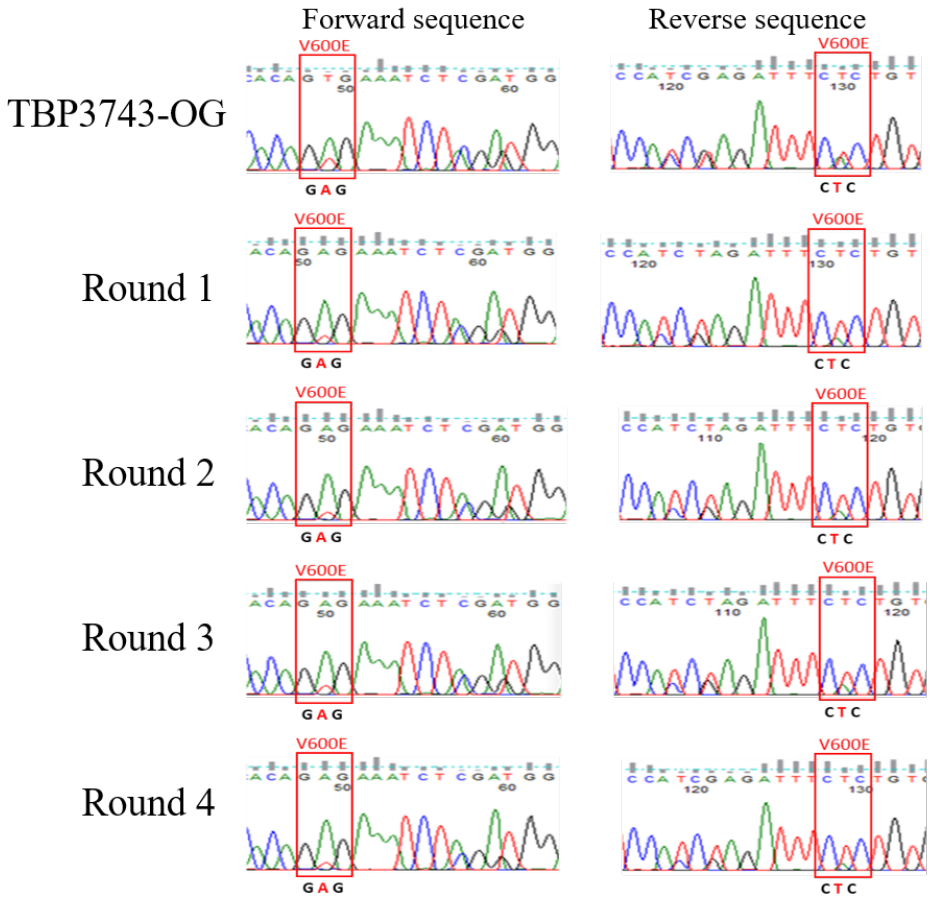

.

Fig 2. Sequencing of BrafV600E mutation.

Identification of BrafV600E mutation during in vivo serial passaging.

Figure 3

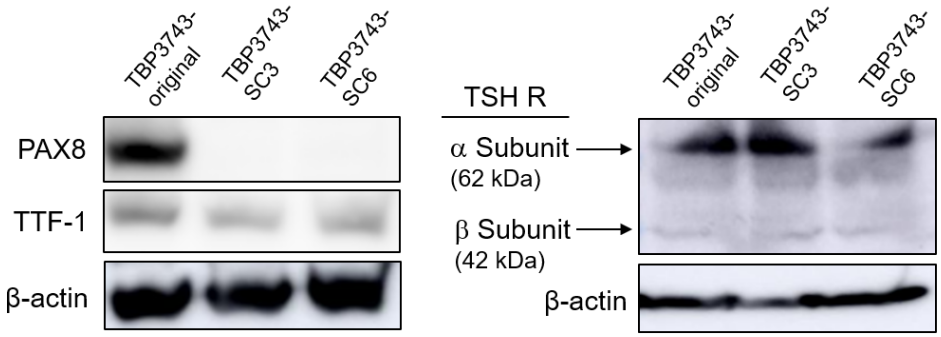

Fig 3. Comparisons of thyroid differentiation markers between original and adapted TBP3743 cells.

The expressions of thyroid differentiation markers (PAX8, TTF-1, TSHR) in TBP3743-original, -adapted (SC3), or -SC6 cells were analyzed by Western blotting. Antibodies specific to PAX8 (1:1000, Invitrogen, MA1-117), TTF-1 (1:1000, Santa cruz, sc-53136), TSHR (1:1000, Santa cruz, sc-53542), and β-actin (used as a loading control) were employed for this analysis.

Figure 4

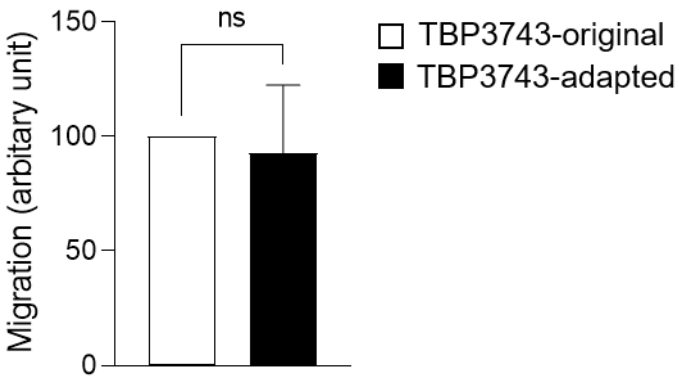

Fig 4. Comparisons of cell migration potentials between original and adapted TBP3743 cells.

Quantitative analysis of transwell cell migration assay. TBP3743-original or -adapted cells (10^5 cells/well) were inserted in upper chambers of transwell migration system and incubated for 12 hours

Figure 5

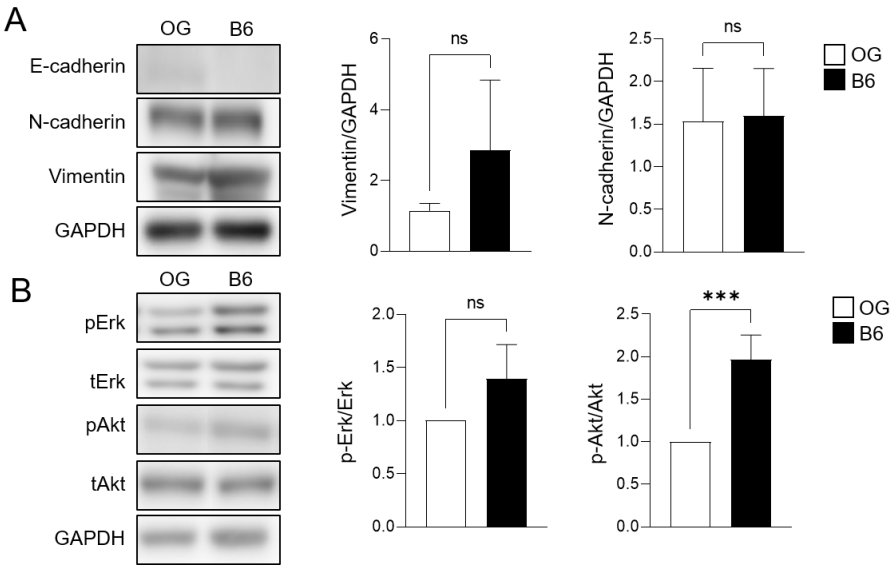

Fig 5. Comparisons of epithelial-mesenchymal markers and oncogenic signalings between original and adapted TBP3743 cells.

(A) Protein expressions of epithelial-mesenchymal markers (E-cadherin, N-cadherin, and Vimentin) in TBP3743-original and -adapted (SC3) cells were analyzed by Western blotting. Antibodies specific to E-cadherin (1:1000, Cell Signaling, #3195), N-cadherin (1:1000, Cell Signaling, #14215), Vimentin (1:1000, Cell Signaling, #5741), and GAPDH (used as a loading control) were employed for this analysis. (B) Phosphorylation status of oncogenic signaling (ERK and AKT) were accessed by Western blot analysis. Antibodies specific to p-Erk (1:1000, Cell Signaling, 9101S), Erk (1:1000, Cell Signaling, 9101S), p-Akt (1:1000, Cell Signaling,

9271S), Akt (1:1000, Cell Signaling, 9272S), and GAPDH (used as a loading control) were employed for this analysis.

Table 1

The number of measurable tumors according to the round of in vivo passing

	Days after tumor cell injection			
	7	14	21	28
Round 1	-/5	-/5	-/5	1/5 (20%)
Round 2	-/5	-/5	1/5 (20%)	3/5 (60%)
Round 3	2/5 (40%)	4/5 (80%)	5/5 (100%)	5/5 (100%)
Round 4	1/5 (20%)	5/5 (100%)	5/5 (100%)	5/5 (100%)

Measurable tumors were defined as a tumor size over 400 mm^2 *in vivo*.

Establishment of an orthotopic tumor model using adapted TBP3743 cells

Orthotopic tumor growth was investigated two weeks after tumor cell injection. The mean volume and weight of tumors collected from the adapted/129 group was greater than that of the original/129 group (volume: 343.8 ± 179.2 mm^3 vs. 599.1 ± 278.9 mm^3, $P < 0.05$; weight: 0.33 ± 0.19 g vs. 0.55 ± 0.22 g, $P < 0.05$, respectively; **Fig. 6A**). The Ki−67^+ cell fraction was markedly higher in the adapted/129 group than the original/129 group (**Fig. 6B and 6C**). Histological features were similar among the groups, presenting with spindle sarcoma−like tumor cells with pleomorphic nuclei and high mitotic count, which are consistent with ATC features (**Fig. 6B**). Hence, the adapted TBP3743 cells exhibited more proliferative characteristics than the original cells in the B6129SF1 mice. However, the tumor volume, weight, and Ki−67^+ cell fraction from the adapted/B6 group were considerably lower than those from the adapted/129 group. Additionally, the median survival was significantly shorter in the original/129 group compared to those of the adapted/B6 group (median [range], 13.5 [11−14] vs 16.5 [5−24] days, P=0.014, **Fig. 6D**)

Figure 6

A.

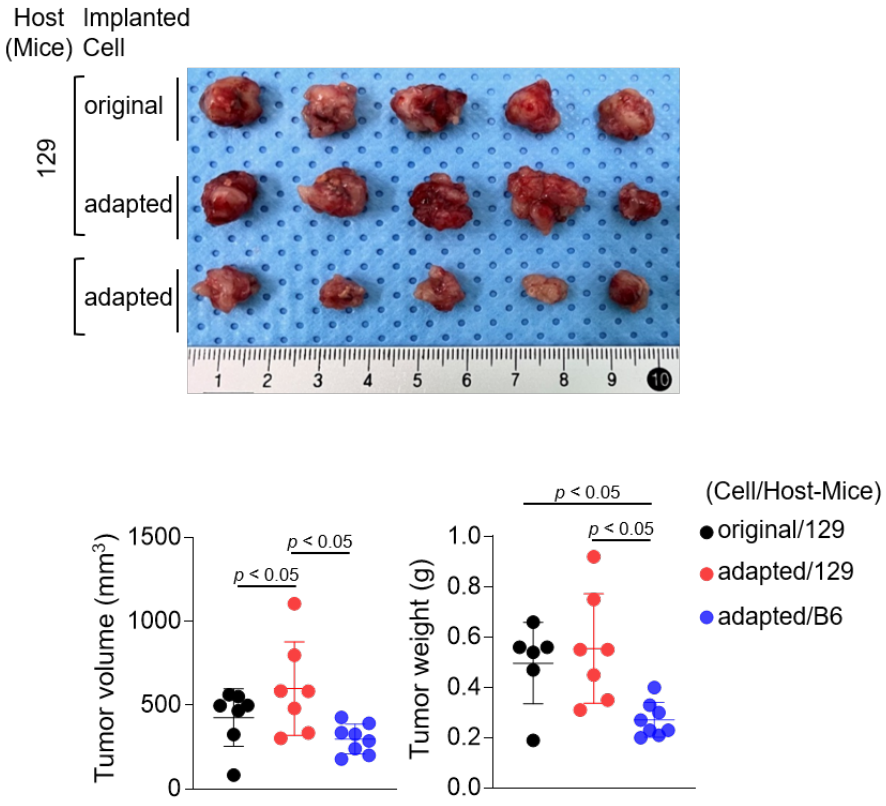
Host (Mice)
Implanted Cell
129
original
adapted
adapted
1 2 3 4 5 6 7 8 9 10
Tumor volume (mm3)
1500
1000
500
0
p < 0.05
p < 0.05
Tumor weight (g)
1.0
0.8
0.6
0.4
0.2
0.0
p < 0.05
p < 0.05
(Cell/Host-Mice)
original/129
adapted/129
adapted/B6

B.

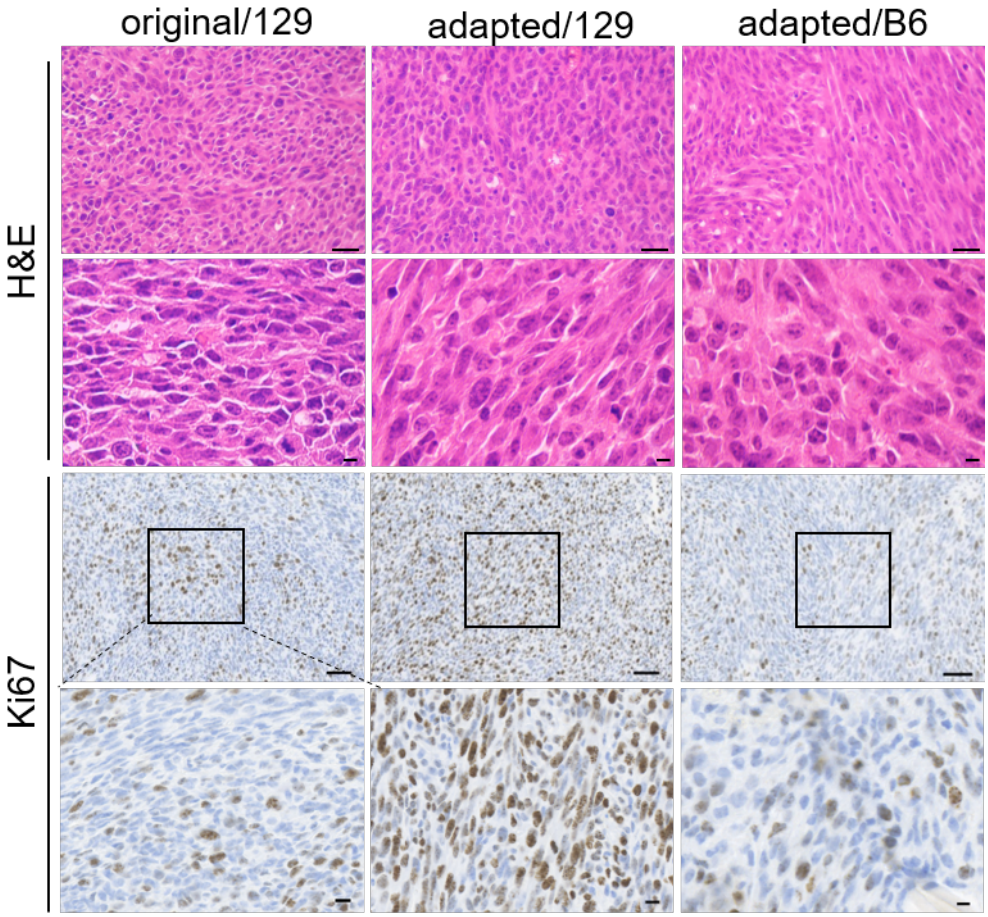
original/129
adapted/129
adapted/B6
H&E
Ki67

C.

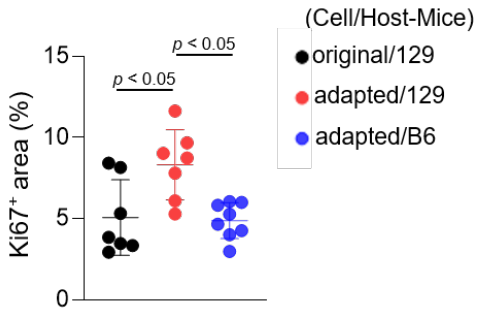
(Cell/Host-Mice)
original/129
adapted/129
adapted/B6
p < 0.05
p < 0.05
Ki67⁺ area (%)
15
10
5
0

D.

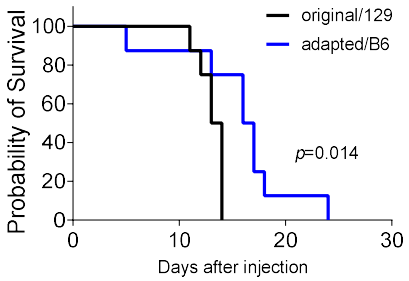

Figure 6. Establishment of orthotopic tumor model using TBP3743-B6 cells.

B6129SF1 mice were implanted with 105 cells of each cell lines (TBP3743-original and -adapted cells) and C57BL/6 mice were implanted with 105 cells of TBP3743-adapted. After 14 days post-implantation, tumors were harvested. (A) Representative image of tumors and, quantification of tumor volume and weight. (B) Representative image of H&E staining and Ki67 immunohistochemistry staining on each tumors (H&E upper panel scale bars: 50 μm; lower panel scale bars: 10 μm; Ki67 panel scale bar: 50 μm; lower panel scale bars: 10 μm). (C) Quantification of Ki67+ area in tumors. (D) FACS analysis of MHC class 1 on TBP3743-original, -adapted, and SC6 tumors. 129, B6129SF1; B6, C57BL/6. All data are expressed as mean ± SD.

Molecular characteristics of adapted TBP3743 cell-derived orthotopic tumors

To investigate the molecular characteristics of each orthotopic tumor, total RNA sequencing analysis was performed on the tumor tissues. Compared to the original/129 group, the adapted/129 and adapted/B6 groups exhibited many DEGs. Meanwhile, a relatively small number of DEGs were detected between the adapted/129 and adapted/B6 groups (**Fig. 7A**).

Gene sets involved in oncogenic signaling, including *Raf,* V*egf-a*, and *Akt,* were highly enriched in the adapted/129 and adapted/B6 groups compared with those in the original/129 tumors (**Fig. 7B** and **7C**). In a similar vein, the activities of gene sets in tumor suppressor signalings, such as *Pten* and *P53*, were attenuated (**Fig. 7B** and **7D**). Furthermore, gene sets associated with epithelial and mesenchymal stem cell proliferation and cell migration were significantly enriched in the adapted/129 and adapted/B6 groups compared with those in the original/129 group **(Fig. 7E and 7F)**. Hence, the oncogenic properties in the adapted cells were more enhanced than the original cells, resulting in more aggressive tumor features.

Figure 7

A.

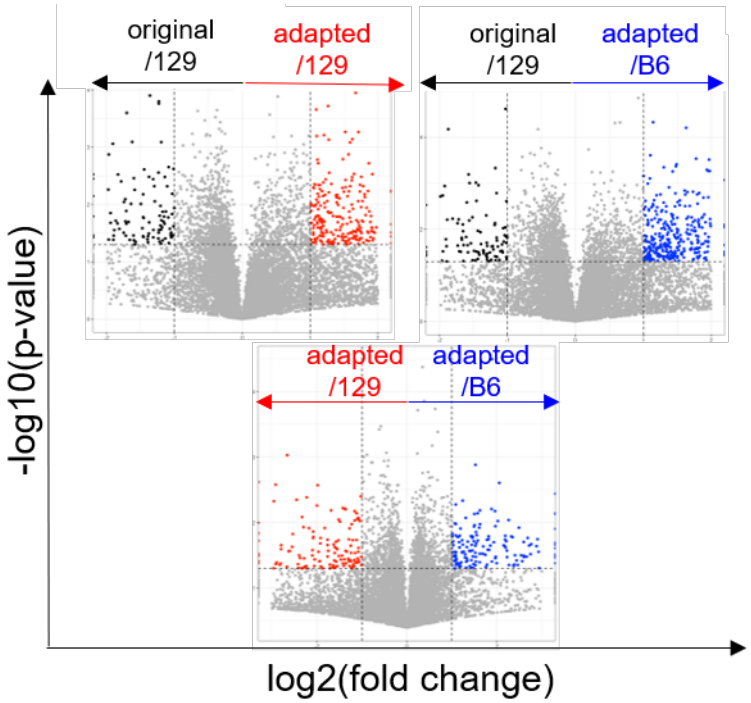
original
/129
adapted
/129
original
/129
adapted
/B6
adapted
/129
adapted
/B6
-log10(p-value)
log2(fold change)

B.

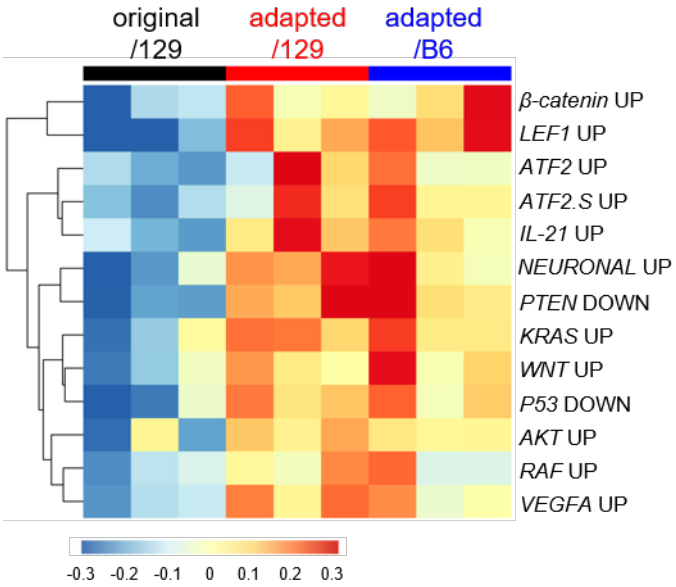
original /129
adapted /129
adapted /B6
β-catenin UP
LEF1 UP
ATF2 UP
ATF2.S UP
IL-21 UP
NEURONAL UP
PTEN DOWN
KRAS UP
WNT UP
P53 DOWN
AKT UP
RAF UP
VEGFA UP
-0.3 -0.2 -0.1 0 0.1 0.2 0.3

C.

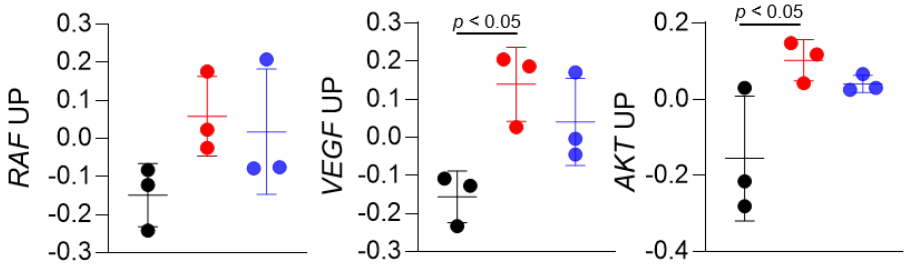
RAF UP
VEGF UP
AKT UP
p < 0.05
p < 0.05

D.

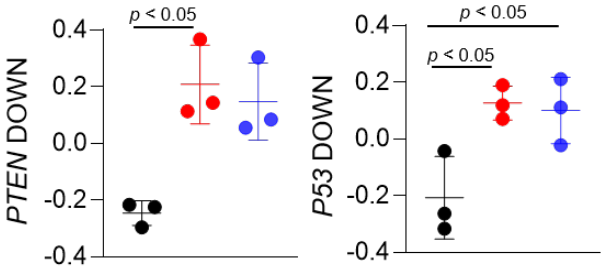
PTEN DOWN
P53 DOWN
p < 0.05
p < 0.05
p < 0.05

E.

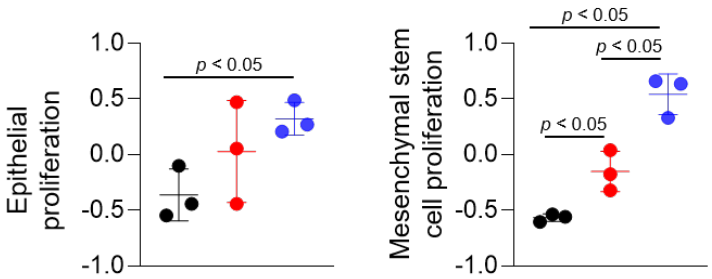
Epithelial proliferation
Mesenchymal stem cell proliferation
p < 0.05
p < 0.05
p < 0.05

F.

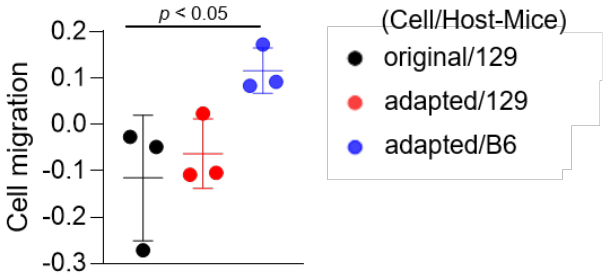
Cell migration
p < 0.05
(Cell/Host-Mice)
original/129
adapted/129
adapted/B6

Figure 7. Molecular characteristics of orthotopic tumors from the adapted TBP3743 cells. B6129SF1 mice were implanted with 10^5 cells of each cell lines (TBP3743-original and -adapted cells) and C57BL/6 mice were implanted with 10^5 cells of TBP3743-adapted. After 14 days post-implantation, tumors were harvested. Total RNA was harvested from whole tumor lysates and sequenced. (A) Volcano plots showing changes of gene expression. (B) Heatmap of changes in oncogenic signaling pathways and (C, D) each of oncogenic pathways. (E) Proliferation of epithelial and mesenchymal stem cells and (F) cell migration analysis. 129, B6129SF1; B6, C57BL/6. All data are expressed as mean ± SD.

Molecular characteristics of the immune microenvironment in adapted TBP3743 cell-derived orthotopic tumors

The next analysed RNA sequencing data to compare the tumor microenvironments among the groups. Notably, immune-related pathways were over-represented in the up-regulated DEGs of the adapted/129 and adapted/B6 groups compared with those of the original/129 group (**Fig. 8A**). Network analysis of the over-represented gene sets further revealed that immune-related pathways were closely organized according to their mutual overlap (**Fig. 8B**). Specifically, heatmap analysis demonstrated that the gene sets related to adaptive (T and B cells) and innate (NK T cells and cytokine production) immune responses were upregulated in the adapted/129 or adapted/B6 group compared with those in the original/129 group (**Fig. 8C**). That is, immune response to tumor cells and immune inhibitory signalling pathways were enriched in the adapted/B6 group compared to that in the original/129 group (**Fig. 8D**). Among the immune checkpoint related genes, both immune stimulatory (*Il2rb* and *Cd28*) and inhibitory (*Ctla4* and *Pdl1*) genes were significantly up-regulated in the adapted/129 or adapted/B6 groups compared with those in the original/129 group

(Fig. 8E). Moreover, RT-PCR analysis revealed that, *in vitro*, stimulatory immune checkpoint genes were down-regulated in the adapted cells compared with the original TBP3743 cells (Table 2). In contrast, *in vivo,* these genes were upregulated in the adapted/B6 tumors compared to original/129 tumors (Fig. 8E). Meanwhile, inhibitory immune checkpoint genes were significantly up-regulated in the adapted cells compared to the original TBP3743 cells (Table 2),
as well as in the adapted/B6 tumors compared with the original/129 tumors (Fig. 8E). Collectively, the immune responses were highly activated in the adapted/129 and adapted/B6 groups compared with those in the original/129 group.

In the comparison between the adapted/129 and adapted/B6 groups, while it could not be statistically assessed, the fold enrichments were higher in the adapted/B6 group (Fig. 8A). More over-represented gene sets from the adapted/B6 participated in the network compared with those of the adapted/129 group (Fig. 8B). Moreover, the expression of *Pdl1* was considerably higher in the adapted/B6 group than in adapted/129 group. The anti-tumor immune responses might be more enhanced in the adapted/B6 group compared with the adapted/129 group.

To validate the distinctive immune characteristics observed

in the adapted TBP3743 cell-derived orthotopic tumors, particularly with regard to tumor-T cell immune interactions, additional *in vivo* experiments were conducted under two immune-modifying conditions. Firstly, athymic nude mice, lacking T cell populations including $CD4^+$ and $CD8^+$ T cells, were utilized to investigate the impact of tumor-T cell interaction on tumor growth. Surprisingly, observed comparable tumor volumes and weights between the original and adapted cell groups over the 9-day period following tumor cell injection (**Fig. 9**). These findings indicate the pivotal role of T cells in the tumorigenesis of the adapted model.

To further investigate the interplay between tumor cells and T cells in the adapted model microenvironment, proceeded with a comparison of the anti-tumor efficacy of an anti-PD-L1 antibody between the original/129 group and the adapted/B6 group. Consistent with a previous study (20), treatment with the anti-PD-L1 antibody alone did not demonstrate a significant treatment response in the original model (**Fig. 8F**). However, in the adapted model, both tumor volume and weight were significantly reduced by 60% and 55%, respectively (**Fig. 8G**). This finding aligns with the gene expression data presented in Fig. 8E, which reveals an upregulation of immune checkpoint modifying genes in the adapted model.

Figure 8

A.

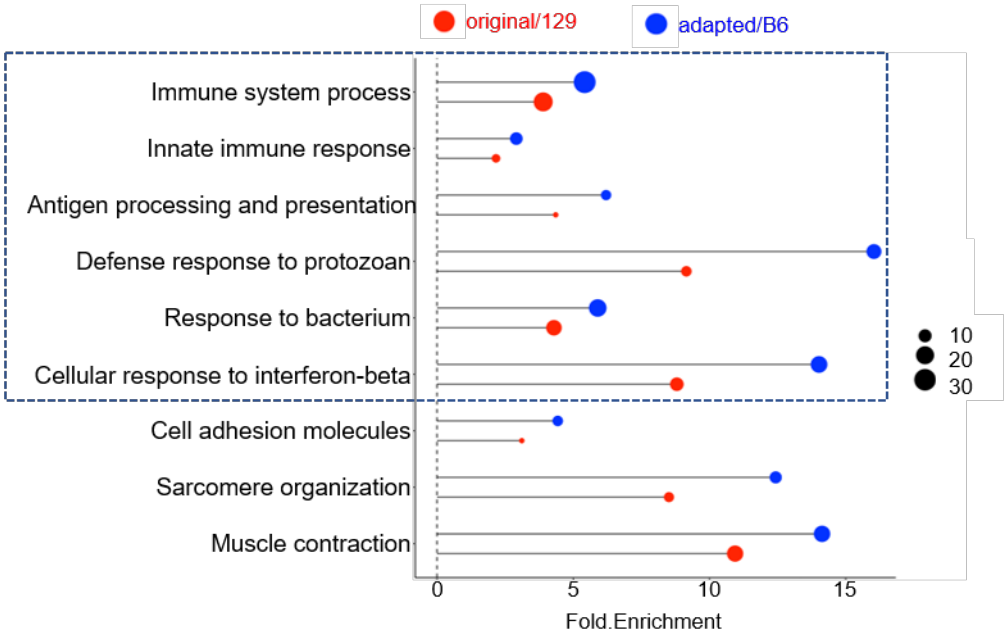
original/129
adapted/B6
Immune system process
Innate immune response
Antigen processing and presentation
Defense response to protozoan
Response to bacterium
Cellular response to interferon-beta
Cell adhesion molecules
Sarcomere organization
Muscle contraction
10
20
30
0
5
10
15
Fold.Enrichment

B.

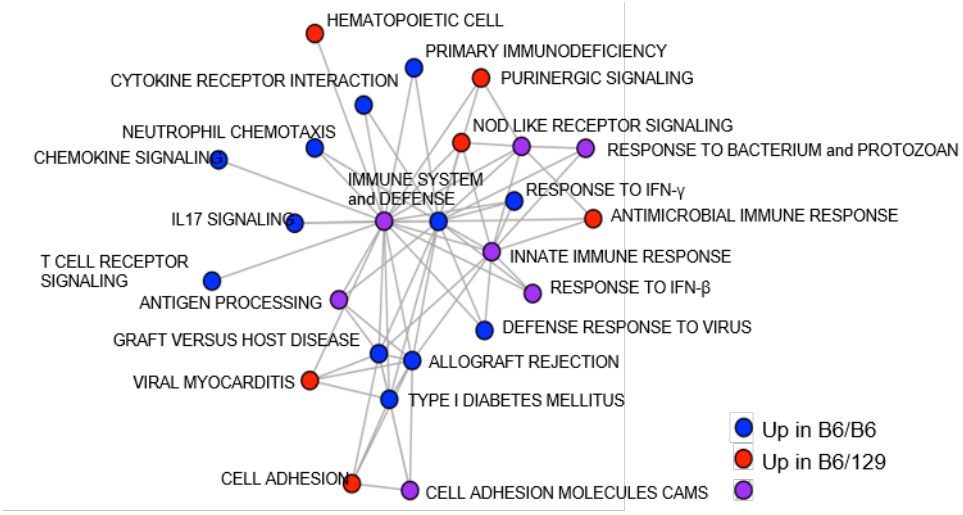
HEMATOPOIETIC CELL
PRIMARY IMMUNODEFICIENCY
CYTOKINE RECEPTOR INTERACTION
PURINERGIC SIGNALING
NEUTROPHIL CHEMOTAXIS
NOD LIKE RECEPTOR SIGNALING
CHEMOKINE SIGNALING
RESPONSE TO BACTERIUM and PROTOZOAN
IMMUNE SYSTEM and DEFENSE
RESPONSE TO IFN-γ
IL17 SIGNALING
ANTIMICROBIAL IMMUNE RESPONSE
INNATE IMMUNE RESPONSE
T CELL RECEPTOR SIGNALING
RESPONSE TO IFN-β
ANTIGEN PROCESSING
DEFENSE RESPONSE TO VIRUS
GRAFT VERSUS HOST DISEASE
ALLOGRAFT REJECTION
VIRAL MYOCARDITIS
TYPE I DIABETES MELLITUS
Up in B6/B6
Up in B6/129
CELL ADHESION
CELL ADHESION MOLECULES CAMS

C.

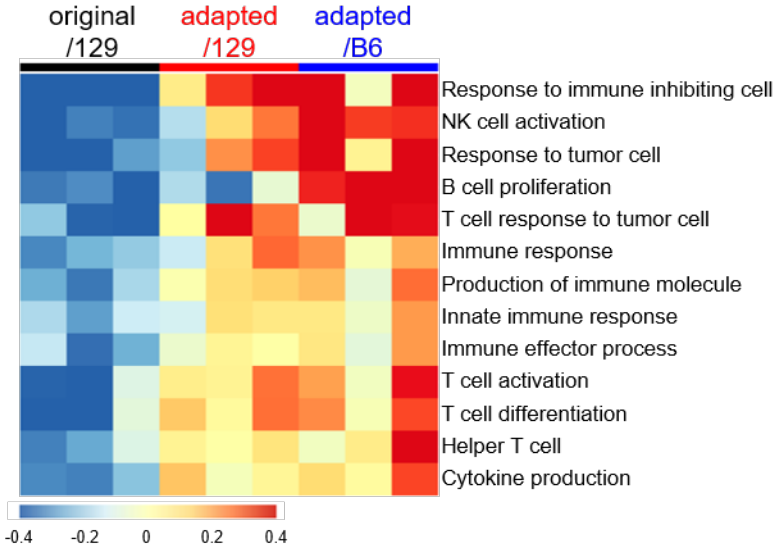
original /129
adapted /129
adapted /B6
Response to immune inhibiting cell
NK cell activation
Response to tumor cell
B cell proliferation
T cell response to tumor cell
Immune response
Production of immune molecule
Innate immune response
Immune effector process
T cell activation
T cell differentiation
Helper T cell
Cytokine production
-0.4
-0.2
0
0.2
0.4

D.

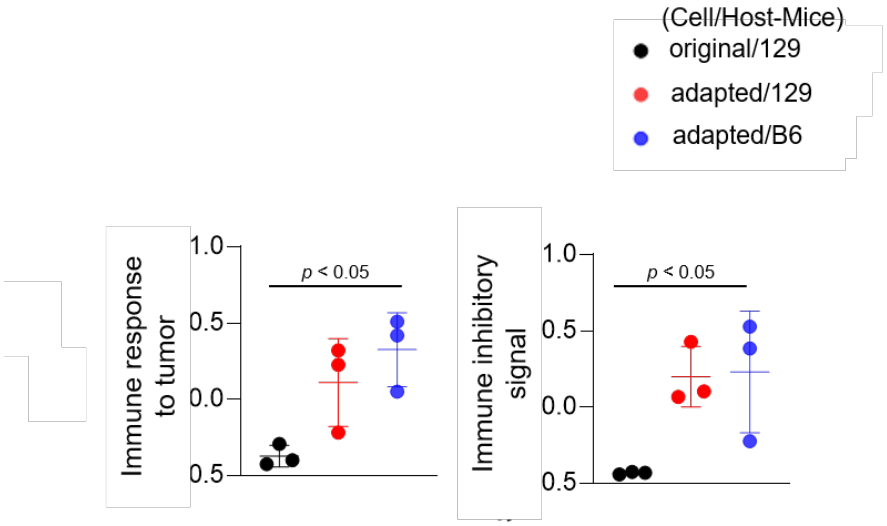
(Cell/Host-Mice)
original/129
adapted/129
adapted/B6
Immune response to tumor
Immune inhibitory signal
p < 0.05
p < 0.05
1.0
0.5
0.0
0.5
1.0
0.5
0.0
0.5

E.

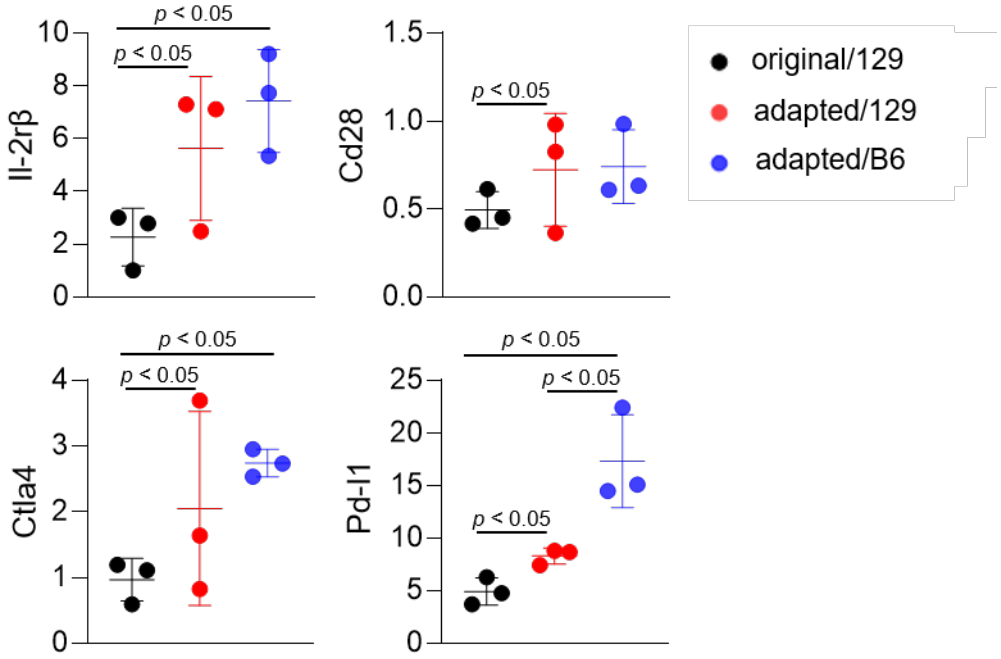
original/129
adapted/129
adapted/B6
Il-2rβ
Cd28
Ctla4
Pd-l1
p < 0.05
p < 0.05
p < 0.05
p < 0.05
p < 0.05
p < 0.05
10
8
6
4
2
0
1.5
1.0
0.5
0.0
4
3
2
1
0
25
20
15
10
5
0

F.

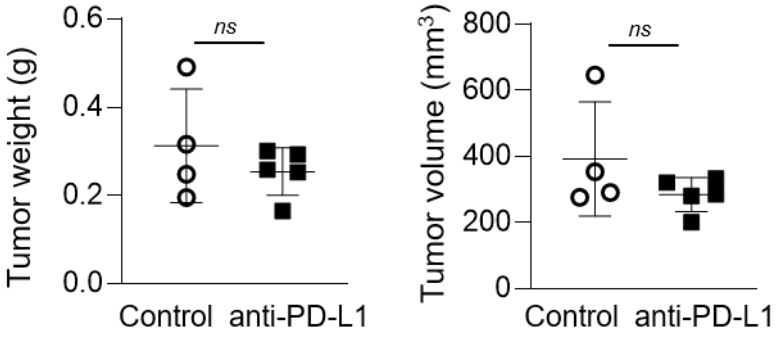

G.

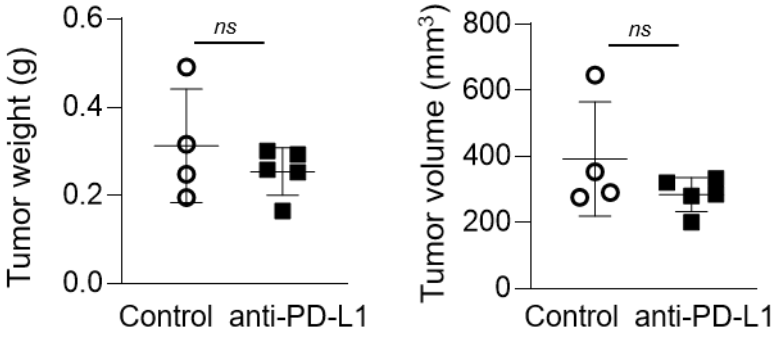

Figure 8. Molecular characteristics of the immune microenvironment in adapted TBP3743 cell-derived orthotopic tumors.

B6129SF1 mice were implanted with 105 cells of each cell lines (TBP3743-original and -adapted cells) and C57BL/6 mice were implanted with 105 cells of TBP3743-adapted. After 14 days post-

implantation, tumors were harvested. Total RNA was harvested from whole tumor lysates and sequenced. (A) Classification of gene set enrichment analysis and (B) the networking of enriched pathways of immune category. (C) Heatmap of changes in immune response signaling pathways and (D) change of immune response to tumor and change of immune inhibitory signal. (E) Alteration of immune stimulatory related marker and immune inhibitory related marker. (F) B6129SF1 mice were implanted with 105 cells of TBP3743-original cells. After 10 days post-implantation, tumors were harvested. Anti-PD-L1 (0.2 mg/kg) was intraperitoneally injected from 5 days after tumor cell injection. Quantification of tumor volume and weight. (G) C57BL/6 mice were implanted with 105 cells of TBP3743-adapted cells. After 10 days post-implantation, tumors were harvested. Anti-PD-L1 (0.2 mg/kg) was intraperitoneally injected from 5 days after tumor cell injection. Quantification of tumor volume and weight. 129, B6129SF1; B6, C57BL/6. All data are expressed as mean ± SD.

Figure 9

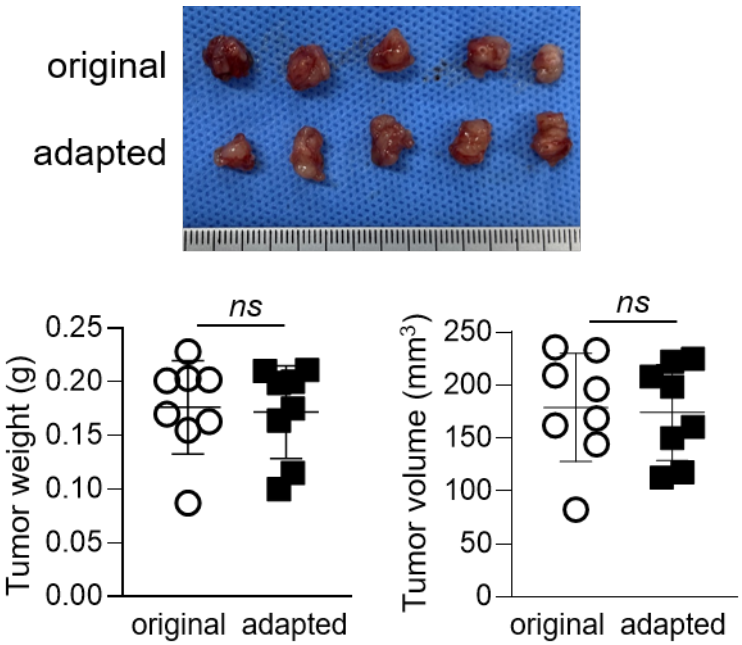

Fig 9. Comparisons of tumorigenicity between original and adapted TBP3743 cells in T cell-deficient mice.

Athymic BALB/c nu/nu mice were implanted with 10^5 cells of both TBP3743-original and TBP3743-adapted cells via orthotopic intrathyroidal injection. Tumors were harvested 9 days after injection, and representative images of in vivo tumors were captured. Tumor volume and weight were quantified.

Table 2

List of genes for RT-qPCR

	Gene	Fold change (OG vs B6)
Thyroid differentiation	*Tshr*	0.38 ± 0.12*
	Pax8	0.01 ± 0.01*
	Ttf-1	0.41 ± 0.18*
	Nis	0.46 ± 0.21*
	Glut1	1.20 ± 0.37
Immune stimulatory	*Il-2rβ*	0.23 ± 0.18*
	Cd40	1.92 ± 0.23
	Tnfrsf18	0.75 ± 0.21
	Tnfrsf4	0.94 ± 0.26
	Tnfrsf9	1.87 ± 0.59
	Cd28	0.23 ± 0.11*
Immune inhibitory	*Pdcd1*	3.30 ± 1.04*
	Pdcdilg2	8.70 ± 1.98*
	Havcr2	6.69 ± 1.51*
	Ctla4	14.98 ± 9.82*
	Pd-l1	1.57 ± 0.01*
	Lag3	0.94 ± 0.38
	Vtcn1	11.61 ± 2.14*
	Cd276	1.31 ± 0.20
	Adora2a	1.74 ± 1.37

*$P < 0.05$

Immune cell profiling of the orthotopic tumor microenvironment

To validate RNA sequencing results, flow cytometric analysis was performed. The $CD45^+$ immune cell fraction was significantly greater in the adapted/B6 group compared with the original/129 group (39.1 ± 7.1% vs 17.4 ± 5.9%, $P < 0.05$; **Fig. 10A**). While the $CD45^+CD3^+$ T cell fraction did not differ significantly among the three groups, those of $CD45^+CD8^+$ cytotoxic T cells and $CD45^+CD4^+$ helper T cells were significantly higher in the adapted/B6 group compared with the original/129 group (**Fig. 10B**). Additionally, the immune activating M1-macrophage ($CD45^+CD11b^+F4/80^+CD80^+CD206^-$) fraction was significantly larger in the adapted/B6 group compared with the original/129 group (3.5 ± 2.1% vs 0.3 ± 0.3%, $P < 0.05$; **Fig. 10C**), while that of the immune suppressive M2 macrophages ($CD45^+CD11b^+F4/80^+CD80^-CD206^+$) did not differ (**Fig. 10C**). Meanwhile, the immune suppressive monocytic myeloid-derived suppressor cell (M-MDSC) ($CD45^+CD11b^+Ly6C^+Ly6G^-$) fraction was significantly larger in the adapted/B6 group than in the adapted/B6:129 group (10.6 ± 4.7% vs 4.1 ± 0.9%, $P < 0.05$; **Fig. 10D**). Flow cytometric subset analysis for T cell and macrophage in

the original/129, the adapted/B6, and the SC6/B6 also supported this notion. Those immune cell changes observed between the original and adapted model did not differ between the adapted/B6 and SC6/B6 (**Fig. 11**). Collectively, both activating and suppressive immune responses were up-regulated in the adapted/B6 group compared with the original/B6 group. However, these differences were not observed between the original/129 and adapted/129 groups.

In addition to the increased immune infiltrate, especially characterized by increased T cell, immune escape cause by losing major histocompatibility (MHC) class I molecule can be another possible immune response in the process of the adapted cell tumorigenesis. Thus, the expression of MHC class I molecules was further analysed. *In vitro* mRNA expression of MHC class I gene was not lost, rather significantly upregulated in both SC3 and SC6 cells compared with the original cell (**Fig 12A**). Additionally, flow cytometric analysis showed that under interferon-γ stimulation, the functional expression of MHC class I in SC3 cells was comparable to that of original cells, while SC6 cells showed a decrease in interferon-γ-mediated upregulation of MHC class I expression (**Fig 12B**). These results suggest that immune escape through functional loss of MHC class I molecules may contribute to tumorigenesis in

adapted cells, particularly in the later phase (represented by SC6 cells) rather than the early phase (represented by SC3 cells).

A bulk mRNA sequencing-based deconvolution analysis was performed to compare the immune profiles of murine tumor models to those of human ATC harboring BRAF mutation. Table 3 showed baseline characteristics of them (n=8). In the comparisons of fractions in $CD4^+$ T cell, $CD8^+$ T cell, and macrophages, human ATC showed higher $CD4^+$ T cell fractions than the murine tumors (Fig. 10E). Given that heavy infiltration of M2-like macrophage is the characteristics of human ATC (3), M2-like macrophage fraction of human ATC was 16.5% (12.6%-21.1%). Those of the murine tumors were 38.4% (32.3%-44.2%) in the original/129 group, 45.4% (45.3-53.8%) in the adapted/129 group, and 36.3% (36.1%-39.9%) in the adapted/B6 group, which were all higher than that of human ATC.

Figure 10

A.

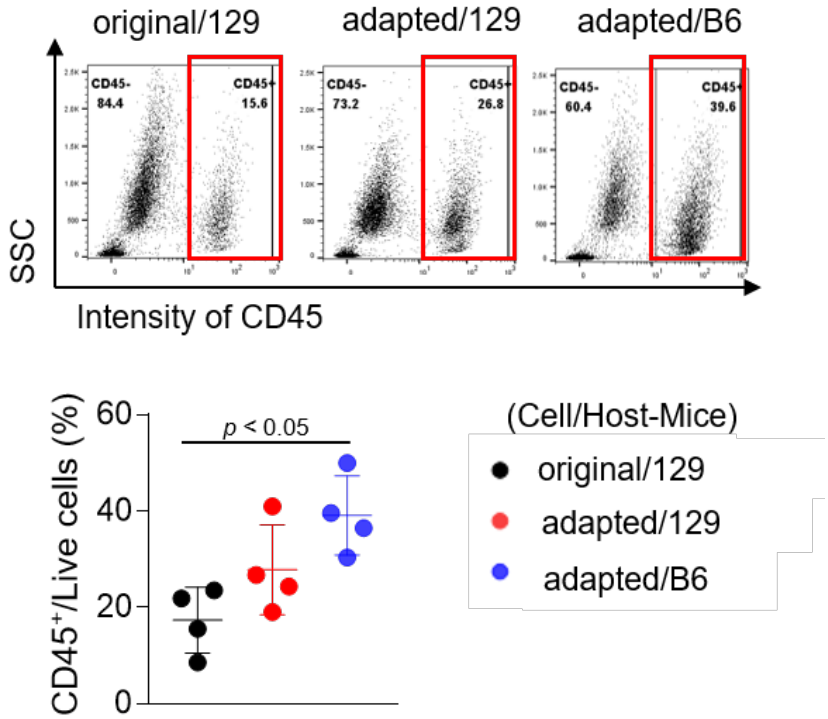
original/129
adapted/129
adapted/B6
CD45-
84.4
CD45+
15.6
CD45-
73.2
CD45+
26.8
CD45-
60.4
CD45+
39.6
SSC
Intensity of CD45
CD45+/Live cells (%)
60
40
20
0
p < 0.05
(Cell/Host-Mice)
original/129
adapted/129
adapted/B6

B.

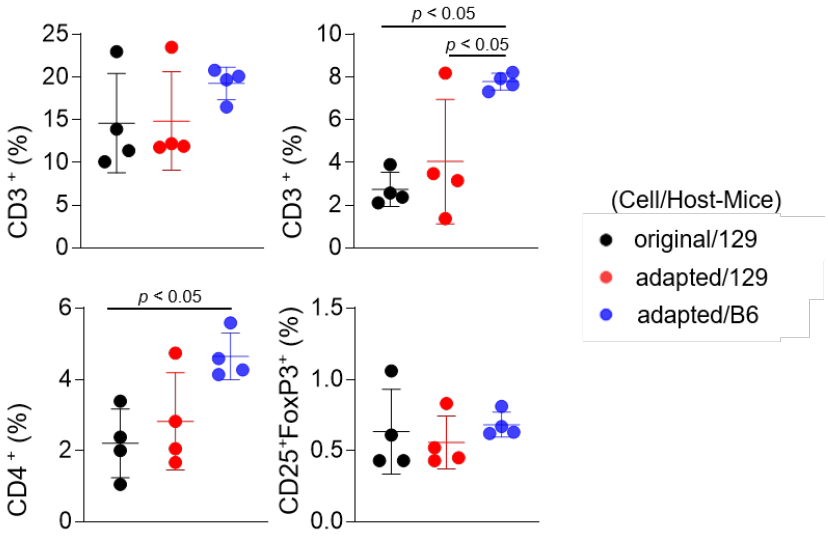
CD3+ (%)
25
20
15
10
5
0
CD3+ (%)
10
8
6
4
2
0
p < 0.05
p < 0.05
CD4+ (%)
6
4
2
0
p < 0.05
CD25+FoxP3+ (%)
1.5
1.0
0.5
0.0
(Cell/Host-Mice)
original/129
adapted/129
adapted/B6

C.

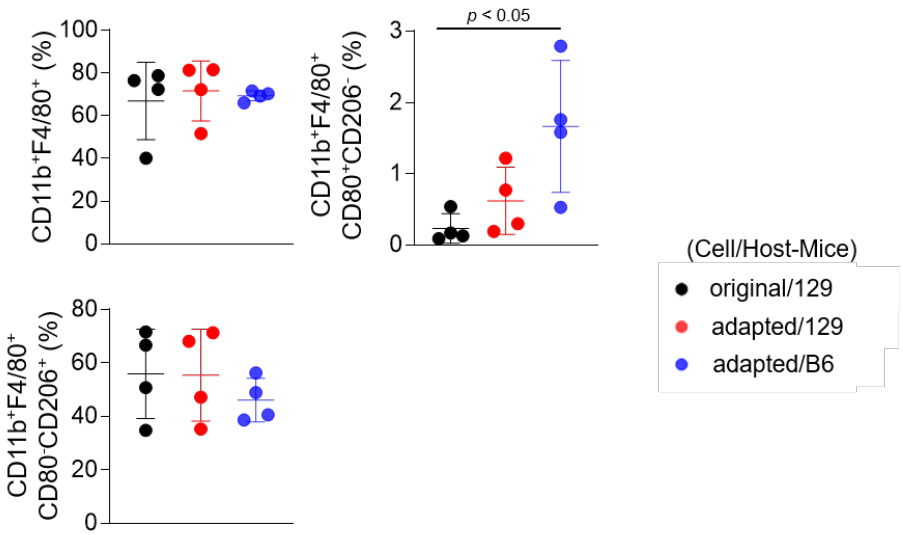
CD11b+F4/80+ (%)
CD11b+F4/80+ CD80+CD206- (%)
p < 0.05
CD11b+F4/80+ CD80-CD206+ (%)
(Cell/Host-Mice)
original/129
adapted/129
adapted/B6

D.

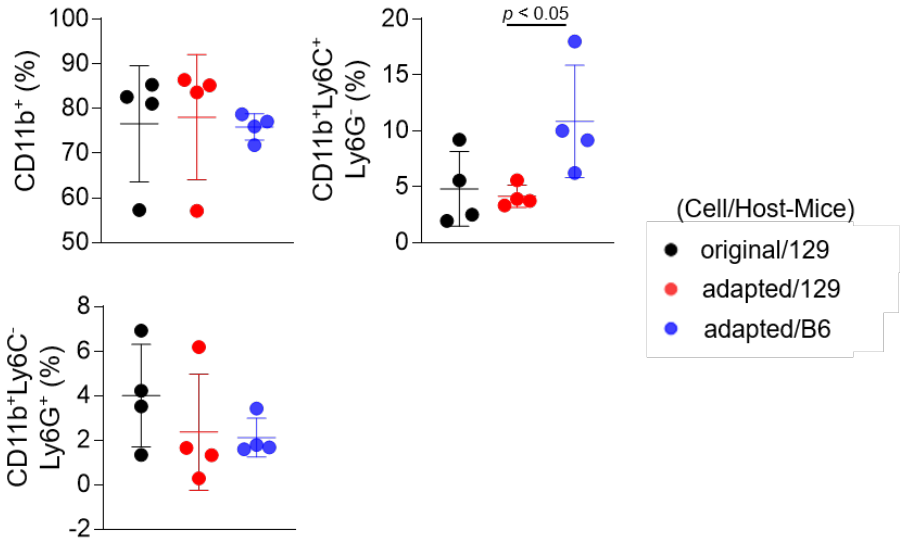
CD11b+ (%)
CD11b+Ly6C+ Ly6G- (%)
p < 0.05
CD11b+Ly6C- Ly6G+ (%)
(Cell/Host-Mice)
original/129
adapted/129
adapted/B6

E.

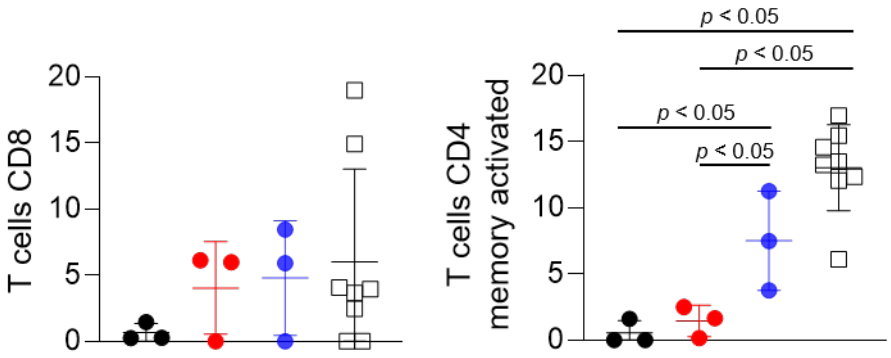
T cells CD8
20
15
10
5
0
T cells CD4 memory activated
p < 0.05
p < 0.05
p < 0.05
p < 0.05

F.

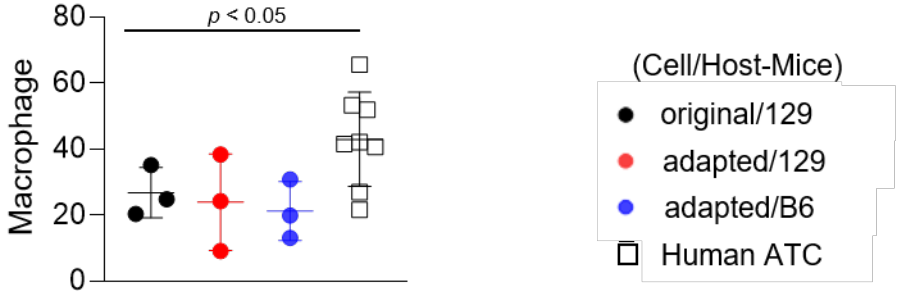
Macrophage
80
60
40
20
0
p < 0.05
(Cell/Host-Mice)
original/129
adapted/129
adapted/B6
Human ATC

Figure 10. Immune cell profiling of the orthotopic tumor microenvironment. B6129SF1 mice were implanted with 10^5 cells of each cell lines (TBP3743−original and −adapted cells) and C57BL/6 mice were implanted with 10^5 cells of TBP3743−adapted. After 14 days post−implantation, tumors were harvested. (A−D) Immune cell fractions were analyzed by flow cytometry analysis using whole tumor lysates. (A) Representative plots and quantified graphs of $CD45^+$ cells in each tumors. Subpopulation of (B) T−lymphocytes ($CD3^+$ pan T; $CD8^+$ cytotoxic T; $CD4^+$ helper T; and $CD25^+FoxP3^+$ regulatory T), (C) macrophages ($CD11b^+F4/80^+$ pan macrophage; $CD11b^+F4/80^+CD80^+CD206^-$ M1−macrophage; and $CD11b^+F4/80^+CD80^-CD206^+$ M2−macrophage), and (D) myeloid cells (CD11b+ pan myeloid; $CD11b^+Ly6C^+Ly6G^-$ M−MDSC; and $CD11b^+Ly6C^-Ly6G^+$ PMC−MDSC). (E−F) RNA sequencing data of 8 human ATC samples were collected from {PMID: 31235699} and deconvolution analysis were performed for comparing immune cell fractions between mice tumors from each group and human ATCs. M−MDSC, mononuclear myeloid−derived suppressor cells; PMN−MDSC, polymorphonuclear myeloid−derived suppressor cells; 129, B6129SF1; B6, C57BL/6. All data are expressed as mean ± SD.

Figure 11

A.

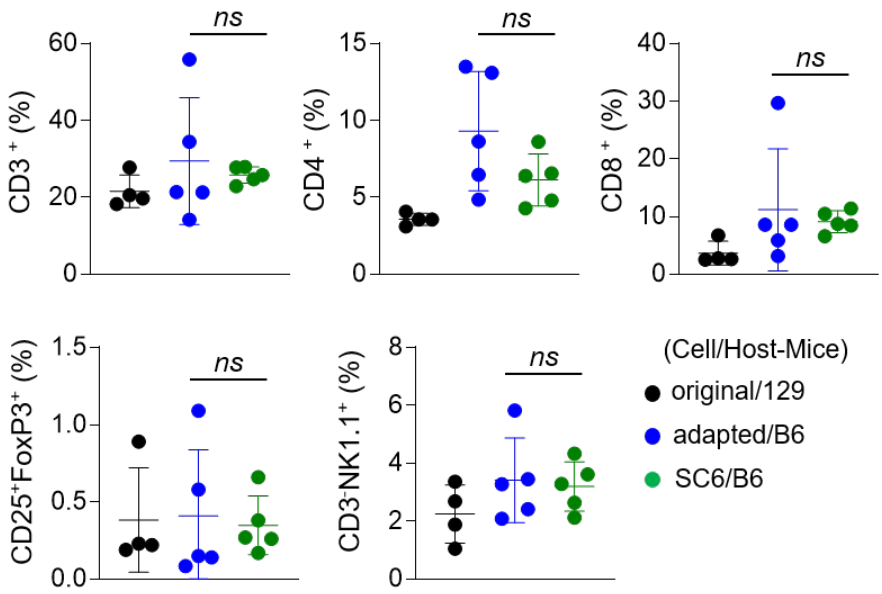
CD3+ (%)
CD4+ (%)
CD8+ (%)
CD25+FoxP3+ (%)
CD3-NK1.1+ (%)
ns
(Cell/Host-Mice)
original/129
adapted/B6
SC6/B6

B.

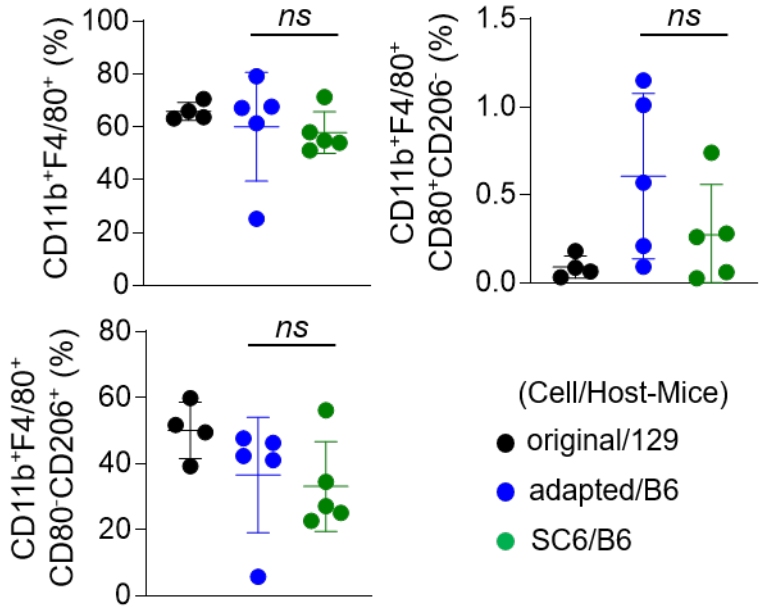
CD11b+F4/80+ (%)
CD11b+F4/80+ CD80+CD206- (%)
CD11b+F4/80+ CD80-CD206+ (%)
ns
(Cell/Host-Mice)
original/129
adapted/B6
SC6/B6

Fig 11. Comparisons of immune cell profiling in tumors between original/129, adapted/B6, and SC6/B6 models.

B6129SF1 mice were implanted with 10^5 cells of TBP3743-original and C57BL/6 mice were implanted with 105 cells of each cell lines (TBP3743-adapted and -SC6 cells). After 14 days post-implantation, tumors were harvested. Immune cell fractions were analyzed by flow cytometry analysis using whole tumor lysates. (A) T-lymphocytes (CD3+ pan T; CD8+ cytotoxic T; CD4+ helper T; CD25+FoxP3+ and regulatory T) and NK cell. (B) Macrophages (CD11b+F4/80+ pan macrophage; CD11b+F4/80+CD80+CD206- M1-like macrophage; and CD11b+F4/80+CD80-CD206+ M2-like macrophage)

Figure 12

A.

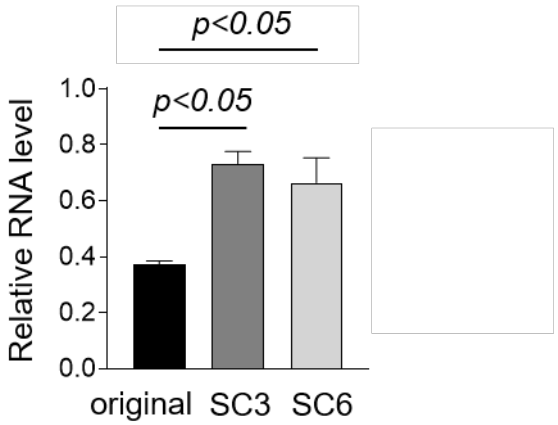
p<0.05
p<0.05
Relative RNA level
1.0
0.8
0.6
0.4
0.2
0.0
original
SC3
SC6

B.

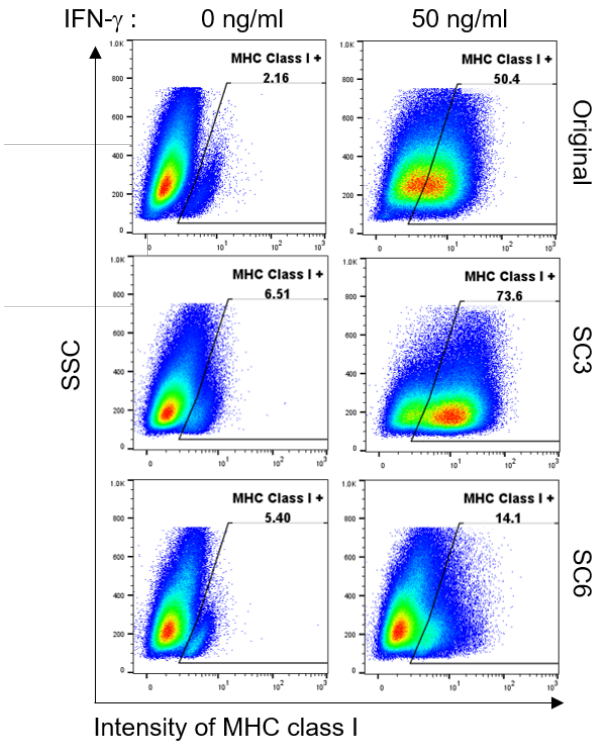
IFN-γ :
0 ng/ml
50 ng/ml
MHC Class I +
2.16
MHC Class I +
50.4
MHC Class I +
6.51
MHC Class I +
73.6
MHC Class I +
5.40
MHC Class I +
14.1
Original
SC3
SC6
SSC
Intensity of MHC class I

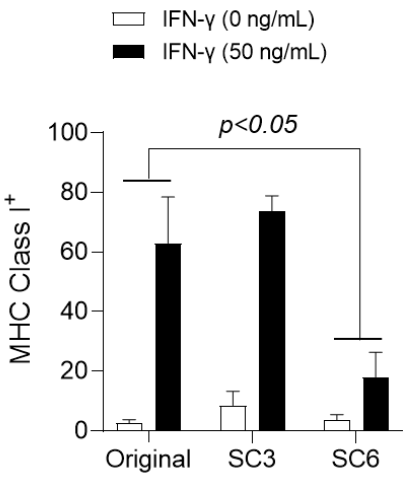

Fig 12. Comparisons of MHC class I expressions in original and adapted TBP3743 cells.

(A) mRNA Expression of MHC class 1 in TBP3743-original, -adapted (SC3), or -SC6 cells were evaluated by RT-PCR analysis. (B) Each cell was stimulated by interferon-γ (50ng/ml) for 24 hours and flow cytometric analysis was performed using anti-mouse MHC class I antibody (1:50, ab95572, Abcam).

Table 3

Clinical characteristics of human ATC

	Human ATC
Number	8
Age, years	71 ± 10.6
Female, n (%)	7 (87.5%)
$BRAF^{V600E}$, n (%)	8 (100%)
TERT promoter mutation, n (%)	8 (100%)
Tumor size, cm	4.5 ± 2.1
Extrathyroidal extension, n (%)	8 (100%)
Lymph node metastasis, n (%)	8 (100%)
Distant metastasis, n (%)	6 (75.0%)
Disease specific death, n (%)	7 (87.5%)

Effects of a BRAF inhibitor on adapted TBP3743 cell-derived orthotopic tumors

Finally, drug responses to PLX-4032, a selective BRAF kinase inhibitor, were explored *in vitro* and *in vivo*. *In vitro,* the inhibitory effects of PLX-4032 on cell viability were similar between the original ($IC_{50,}$ 4.7μM) and adapted ($IC_{50,}$ 3.5μM) cells (**Fig. 13A**). However, PLX-4032 treatment in the adapted/B6 group significantly reduced tumor burden by 84%, as determined by bioluminescence imaging, and tumor weight by 43% compared with the untreated group (**Fig. 13B** and **13C**).

Considering that a previous study reported immune modulatory effects of BRAF kinase inhibitor(20), the T cell and macrophage densities within the tumor microenvironment were assessed by IHC. Consistent with the previous study(20), the $CD3^+$, $CD4^+$, and $CD8^+$ T cell proportions were increased in the PLX-4032-treated group compared to the untreated group (**Fig. 13D**). Moreover, the $F4/80^+$ macrophage proportion exhibited no difference, while that of $CD163^+$ M2-macrophages was decreased (**Fig. 13D**). Collectively, the adapted TBP3743 cells responded to PLX-4032 appropriately, and the adapted/B6 model proved applicable for evaluation of the anti-tumor efficacy and immune

modulatory effects of drugs.

Figure 13

A.

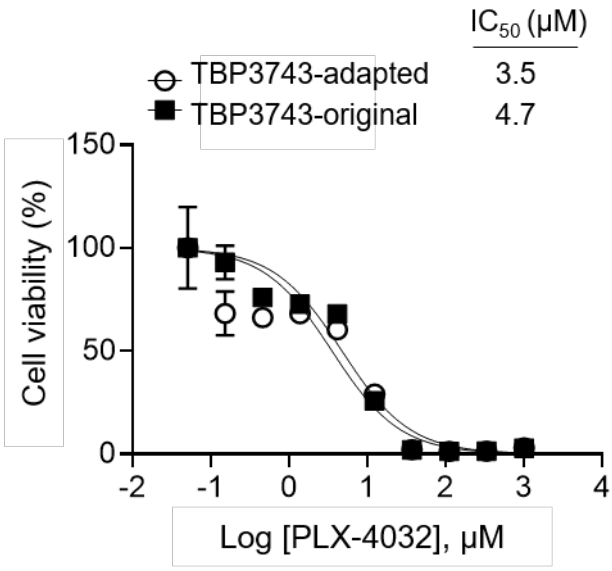
IC50 (μM)
TBP3743-adapted 3.5
TBP3743-original 4.7
Cell viability (%)
150
100
50
0
-2
-1
0
1
2
3
4
Log [PLX-4032], μM

B.

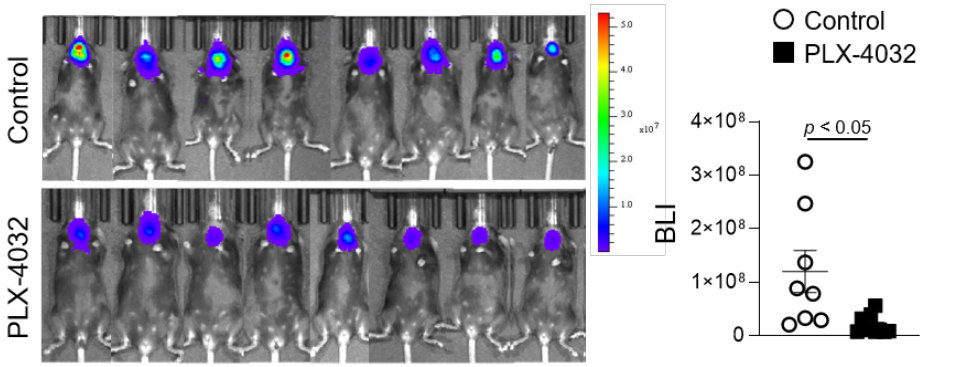
Control
PLX-4032
BLI
Control
PLX-4032
p < 0.05
4×10^8
3×10^8
2×10^8
1×10^8
0

C.

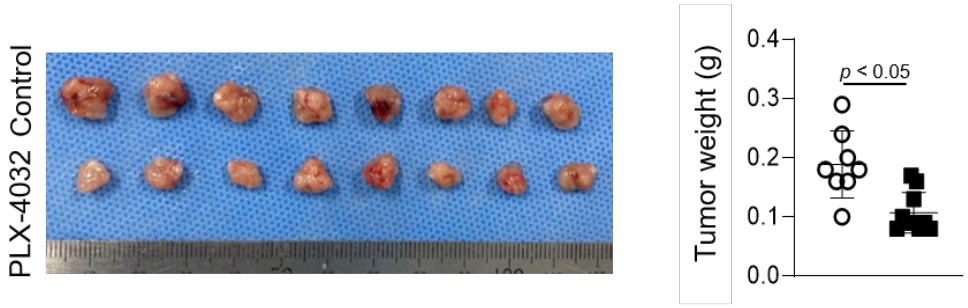
PLX-4032 Control
Tumor weight (g)
p < 0.05
0.4
0.3
0.2
0.1
0.0

D.

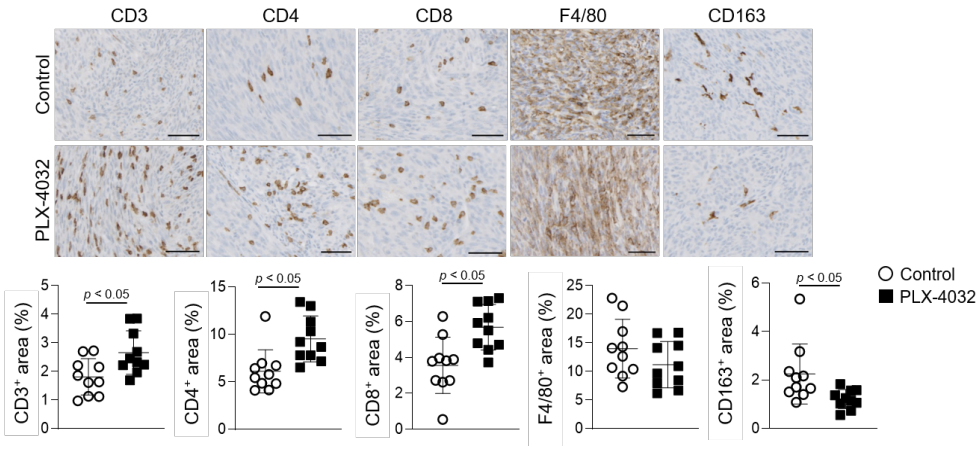
CD3
CD4
CD8
F4/80
CD163
Control
PLX-4032
CD3⁺ area (%)
CD4⁺ area (%)
CD8⁺ area (%)
F4/80⁺ area (%)
CD163⁺ area (%)
p < 0.05
Control
PLX-4032

Figure 13. Effects of *BRAF*^{V600E} inhibitor on adapted TBP3743-B6 cells. (A) Effect of PLX-4032 on TBP3743-original and -adapted cells were measured by cell viability assay. (B-D) TBP3743-adapted cells (1×10^5/10μL PBS) were injected into the murine thyroid via orthotopic injection, and mice were daily treated with 10 mg/kg of PLX-4032. At 2 weeks after injection, tumors were harvested. (B) bioluminescence imaging and (C) representative image of tumors, and quantification of tumor weight. (D) Representative images of IHC for T cell (CD3), helper T cell (CD4), cytotoxic T cell (CD8), macrophage (F4/80), and M2-macrophage (CD163) in each group tumors. scale bars: 50μm. All data are expressed as mean ± SD.

Effects of a Combination therapy on adapted TBP3743 cell-derived orthotopic tumors

Given that Adapted/B6 group displayed increased expression of the immune inhibitory molecule PD-L1 **(Fig. 8E)** and heightened macrophage frequency **(Fig. 10C)**, combination therapy of anti-CD47 and/or immune checkpoint inhibitors with BRAF inhibitor was explored to ascertain its anti-tumor effects. The binding of tumor-associated macrophage antigen CD47 with SIRPα induces a "don't eat me" signal, impeding the macrophage-mediated phagocytosis (24). In the BRAF inhibitor + anti-CD47 (66.3% tumor growth inhibition), BRAF inhibitor + anti-PD-L1 (83.4% tumor growth inhibition) and BRAF inhibitor + anti-CD47 + anti-PD-L1 (82.7% tumor growth inhibition) treatment groups, dramatic tumor reduction was observed compared to the untreated group (**Fig. 14A, B**). Moreover, the combination therapy group showed prolonged survival compared to the untreated group (**Fig. 14C**)

Figure 14

A.

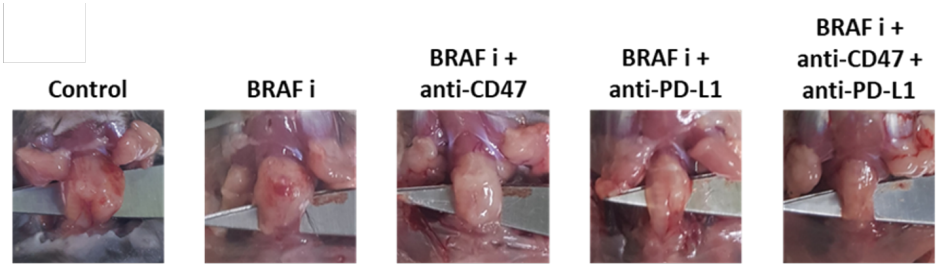
Control
BRAF i
BRAF i +
anti-CD47
BRAF i +
anti-PD-L1
BRAF i +
anti-CD47 +
anti-PD-L1

B.

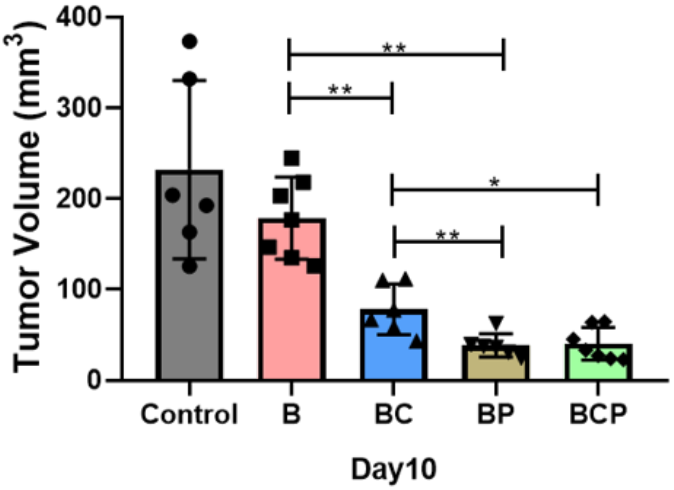
Tumor Volume (mm3)
400
300
200
100
0
**
**
*
**
Control
B
BC
BP
BCP
Day10

C.

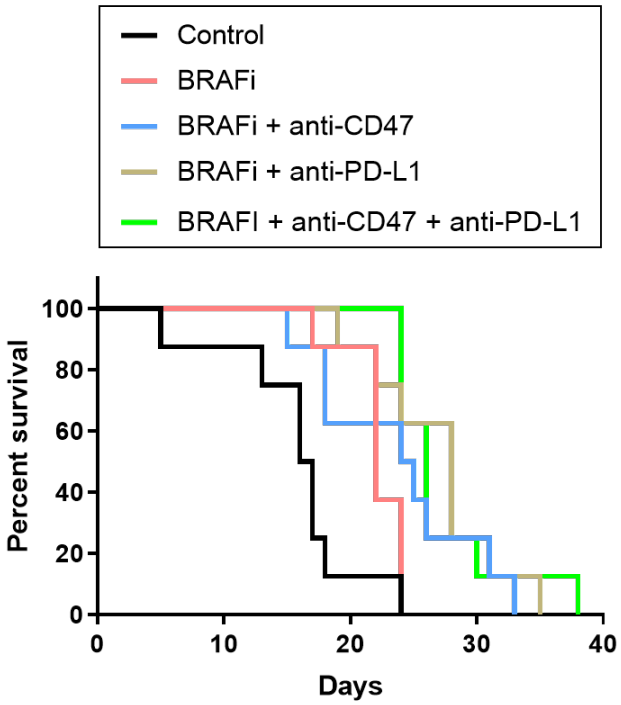
Control
BRAFi
BRAFi + anti-CD47
BRAFi + anti-PD-L1
BRAFI + anti-CD47 + anti-PD-L1
Percent survival
100
80
60
40
20
0
0
10
20
30
40
Days

Figure 14. Combination therapeutic effects of BRAF inhibitor, anti-CD47 and PD-L1 in adapted/B6 tumor model. (A) Gross morphology of tumor after euthanization at 10 days after implantation(1×10^5/10μL PBS). Combination therapy for 1 week led to (B) tumor growth inhibition and (C) prolonged the survival compared to control. (C) Mice survived for a median of 16.5±3 days (control), 22±2 days (PLX-4032), 24.5±10.5 days (PLX-4032 + anti-CD47), 28±6.5 days (PLX-4032 + anti-PD-L1) and 26±4 days (PLX-4032 + anti-CD47 + anti-PD-L1).

Discussion

In the present study, adapted the B6129SF1 mouse-derived ATC cell line, TBP3743, harbouring *Braf*^{V600E} mutation and *Trp53* and *Pten* deletion(19), into C57BL/6 inbred mice and established a novel orthotopic tumor model of ATC. Although the adapted TBP3743 cells were de-dedifferentiated, they exhibited similar gross morphology, cell viability, and migration/invasion potential as the original TBP3743 cells *in vitro*. Moreover, our novel orthotopic tumor model in C57BL/6 mice showed similar histological features to human ATC with high oncogenic properties and activated anti-tumor immune responses. Indeed, the anti-tumor effects and immune modulatory effects of a BRAF inhibitor were observed in the model.

The adapted cells represented de-differentiated clones. During *in vivo* serial passaging, PAX8 expression was completely lost, while the expressions of TTF-1 and TSH-R were low but preserved. In contrast to the typical pattern observed in human ATC, where PAX8 is generally preserved (25, 26) and TTF-1 and TSH-R are lost earlier in the de-differentiation process (27), the TBP3743 cell line used in our study exhibited a different order of gene deletion. The adapted cells showed a reduction in mRNA

expression of *TTF-1* and *TSH-R* compared to the original cells, but preservation of protein expressions of TTF-1, while the protein levels of TSH-R were negligible. Additionally, the recently described ATC marker gene, IGF2BP1 (23), was preserved in both the original and adapted cells. These findings indicate that the adapted ATC cells were still undergoing the de-differentiation process observed in human thyroid cancer.

The histologic features of the original/129, adapted/129, and adapted/B6 cells were consistent with human sarcomatoid ATC, characterized by spindle sarcoma-like tumor cells with pleomorphic nuclei and a high mitotic count. The complete loss of PAX8 in the adapted cells can be explained by previous reports indicating low positivity of PAX8 in human sarcomatoid ATC (less than 50%) (25, 26). Therefore, the adapted cells and the adapted/B6 model, paired with the original cells and original/129 model, provide a valuable tool for investigating the pathophysiology of the de-differentiation process in ATC.

The present study focused on analysing the molecular characteristics of ATC tumors using RNA sequencing data. *In vitro* analysis revealed that the gross cancer cell behaviours, including cell proliferation rates, with or without BRAF inhibitors, or migration/3D invasion potentials, were similar between the original

and adapted cells. However, the rate of *in vivo* tumor growth and the Ki-67 index was significantly higher in B6129SF1 mice injected with the adapted TBP3743 cells compared to those injected with original TBP3743 cells. Molecular analyses supported these phenotypic differences demonstrating that gene sets associated with driver mutation pathways, such as RAF upregulation and PTEN and P53 down-regulation, as well as other oncogenic pathways, were enhanced in the tumors derived from adapted TBP3743 cells compared to original cells in B6129SF1 mice. These findings highlight the marked differences in cancer cell behaviour within *in vivo* and *in vitro* systems; thus, *in vitro* results must be interpreted carefully.

The evaluation of MHC molecule expression provides further insight into the adaptation mechanism studied here. In general, the selected clones exhibited loss of MHC genes, which has the potential to lead to immune evasion. Interestingly, the original cells and SC3 clone, representing an early adapted cell, retained their antigen-presentation functions by expressing MHC class I molecules. However, the SC6 clone exhibited significant loss of functional MHC class I under interferon-γ stimulation, highlighting the critical role of immune evasion in the later stages of the adapted model, while not observed in the early adaptation model. Therefore,

careful selection and optimization of subclone passages are necessary for further study.

Interestingly, the tumor growth rate differed between murine hosts (i.e., B6129SF1 versus C57BL/6), even following implantation of the same adapted TBP3743 cells. The adapted TBP3743 cells enhanced immune responses to tumors in all mice; however, the effect was stronger in C57BL/6 than in B6129SF1 mice. Not only were the immune stimulatory responses, including cytotoxic T cell or M1 macrophage proportions, enhanced in C57BL/6 mice compared to B6129SF1 mice, but also the immune suppressive responses, such as the M-MDSC proportion and *Pdl1* expression. This homeostasis of immune responses might account for the overall reduced tumor growth in C57BL/6 mice compared with B6129SF1 mice. Indeed, these findings highlight the importance of the interactions between the tumor microenvironment and cancer cells. This was further demonstrated *in vitro* by the downregulated expression of immune checkpoint genes in the adapted TBP3743 cells *in vitro,* which became upregulated following *in vivo* generation of tumors within C57BL/6 mice. Hence, cancer cells exhibit dynamic molecular responses to the host immune responses.

ATC stands out among various solid cancers as a highly immunogenic tumor characterized by dense infiltration of tumor-

associated macrophages (TAMs) (3). Additionally, recent single-cell transcriptomics data have demonstrated that the tumor immune microenvironment undergoes significant reprogramming during ATC progression. This reprogramming is initiated by the substantial infiltration of immune cells, including macrophages and T cells, during the anaplastic transformation (28). Hence, understanding cancer-immune cell interactions is crucial in ATC research (29, 30). Our deconvolution analysis of total RNA sequencing data confirms the abundant presence of $CD4^+$ and $CD8^+$ T cells in human ATC samples, consistent with previous studies (31). Notably, the adapted/B6 model closely recapitulates the degree of tumor-infiltrating T cells observed in human ATC samples compared to other murine tumor groups. With the development of various T cell-targeting anti-tumor drugs over the past decade (32-34), some of which have demonstrated success in clinical settings (35-37), our model provides an improved platform for the ongoing advancement of immune-modulating therapeutics for ATC. Specifically, it enables more sensitive verification of the anti-tumor and immune-modulatory effects of candidate drugs in a model that closely mirrors the immune response observed in human ATC. Furthermore, the adapted model's median survival which is approximately 14 days offers an extended timeframe to assess drug

response. Indeed, the adapted model demonstrated a notable response to anti-PD-L1 therapeutics, whereas the original model exhibited limited efficacy, consistent with previous findings (20).

Overall, the pros and cons of the adapted model is summarized as follows. The adapted model is the representative model of human ATC: The adapted cells are de-differentiated, possess molecular characteristics of human ATC. *In vivo* tumor with the adapted cells in C57BL/6 results in heavy infiltration of immune cells, which possibly resembles distinct tumor-host immune interaction of human ATC. The tumor growth rate and median survival is appropriate to investigate responses of anti-tumor drugs. Despite our interpretation that the adapted model represents the characteristics of de-differentiated clones and enhanced immune response similar to "hot tumors" in human ATCs, it is possible that the observed enhanced immunity is partially due to simple allogenic rejection. Additionally, while claimed that the prolonged survival in the adapted model is more suitable for drug development, it may raise concerns that this prolongation conflicts with the features of human ATC. However, it should be noted that the median survival of our model (16.5 days) is significantly shorter than the orthotopic mouse model using the 8505c human ATC cell-line, which showed steady tumor growth over 35 days without any

deaths (38).

In conclusion, a novel orthotopic tumor model of ATC has been established by successful cell adaptation via *in vivo* passage in inbred C57BL/6 mice. This new syngenic ATC mouse model will advance the current understanding of the tumor microenvironment, particularly from an immunological context, and will prove effective as a preclinical platform for ATC drug discovery.

References

1. Simoes-Pereira J, Capitao R, Limbert E, Leite V. Anaplastic Thyroid Cancer: Clinical Picture of the Last Two Decades at a Single Oncology Referral Centre and Novel Therapeutic Options. Cancers (Basel). 2019;11(8).

2. Maniakas A, Dadu R, Busaidy NL, Wang JR, Ferrarotto R, Lu C, et al. Evaluation of Overall Survival in Patients With Anaplastic Thyroid Carcinoma, 2000-2019. JAMA Oncol. 2020;6(9):1397-404.

3. Jung KY, Cho SW, Kim YA, Kim D, Oh BC, Park DJ, et al. Cancers with Higher Density of Tumor-Associated Macrophages Were Associated with Poor Survival Rates. J Pathol Transl Med. 2015;49(4):318-24.

4. Kim DI, Kim E, Kim YA, Cho SW, Lim JA, Park YJ. Macrophage Densities Correlated with CXC Chemokine Receptor 4 Expression and Related with Poor Survival in Anaplastic Thyroid Cancer. Endocrinol Metab (Seoul). 2016;31(3):469-75.

5. Iyer PC, Dadu R, Gule-Monroe M, Busaidy NL, Ferrarotto R, Habra MA, et al. Salvage pembrolizumab added to kinase inhibitor therapy for the treatment of anaplastic thyroid carcinoma. J

Immunother Cancer. 2018;6(1):68.

6. Rao SN, Zafereo M, Dadu R, Busaidy NL, Hess K, Cote GJ, et al. Patterns of Treatment Failure in Anaplastic Thyroid Carcinoma. Thyroid. 2017;27(5):672-81.

7. Landa I, Ibrahimpasic T, Boucai L, Sinha R, Knauf JA, Shah RH, et al. Genomic and transcriptomic hallmarks of poorly differentiated and anaplastic thyroid cancers. J Clin Invest. 2016;126(3):1052-66.

8. Yoo SK, Song YS, Lee EK, Hwang J, Kim HH, Jung G, et al. Integrative analysis of genomic and transcriptomic characteristics associated with progression of aggressive thyroid cancer. Nat Commun. 2019;10(1):2764.

9. Yoo SK, Song YS, Park YJ, Seo JS. Recent Improvements in Genomic and Transcriptomic Understanding of Anaplastic and Poorly Differentiated Thyroid Cancers. Endocrinol Metab (Seoul). 2020;35(1):44-54.

10. Kunstman JW, Juhlin CC, Goh G, Brown TC, Stenman A, Healy JM, et al. Characterization of the mutational landscape of anaplastic thyroid cancer via whole-exome sequencing. Hum Mol Genet. 2015;24(8):2318-29.

11. Subbiah V, Kreitman RJ, Wainberg ZA, Cho JY, Schellens JHM, Soria JC, et al. Dabrafenib and Trametinib Treatment in

Patients With Locally Advanced or Metastatic BRAF V600-Mutant Anaplastic Thyroid Cancer. J Clin Oncol. 2018;36(1):7-13.

12. Subbiah V, Kreitman RJ, Wainberg ZA, Cho JY, Schellens JHM, Soria JC, et al. Dabrafenib plus trametinib in patients with BRAF V600E-mutant anaplastic thyroid cancer: updated analysis from the phase II ROAR basket study. Ann Oncol. 2022;33(4):406-15.

13. Jeon MJ, Haugen BR. Preclinical Models of Follicular Cell-Derived Thyroid Cancer: An Overview from Cancer Cell Lines to Mouse Models. Endocrinol Metab (Seoul). 2022;37(6):830-8.

14. Jin Y, Liu M, Sa R, Fu H, Cheng L, Chen L. Mouse models of thyroid cancer: Bridging pathogenesis and novel therapeutics. Cancer Lett. 2020;469:35-53.

15. Charles RP, Iezza G, Amendola E, Dankort D, McMahon M. Mutationally activated BRAF(V600E) elicits papillary thyroid cancer in the adult mouse. Cancer Res. 2011;71(11):3863-71.

16. Richmond A, Su Y. Mouse xenograft models vs GEM models for human cancer therapeutics. Dis Model Mech. 2008;1(2-3):78-82.

17. Becher OJ, Holland EC. Genetically engineered models have advantages over xenografts for preclinical studies. Cancer Res. 2006;66(7):3355-8, discussion 8-9.

18. McFadden DG, Vernon A, Santiago PM, Martinez-McFaline R, Bhutkar A, Crowley DM, et al. p53 constrains progression to anaplastic thyroid carcinoma in a Braf-mutant mouse model of papillary thyroid cancer. Proc Natl Acad Sci U S A. 2014;111(16):E1600-9.

19. Vanden Borre P, McFadden DG, Gunda V, Sadow PM, Varmeh S, Bernasconi M, et al. The next generation of orthotopic thyroid cancer models: immunocompetent orthotopic mouse models of BRAF V600E-positive papillary and anaplastic thyroid carcinoma. Thyroid. 2014;24(4):705-14.

20. Gunda V, Gigliotti B, Ndishabandi D, Ashry T, McCarthy M, Zhou Z, et al. Combinations of BRAF inhibitor and anti-PD-1/PD-L1 antibody improve survival and tumour immunity in an immunocompetent model of orthotopic murine anaplastic thyroid cancer. Br J Cancer. 2018;119(10):1223-32.

21. Song HK, Hwang DY. Use of C57BL/6N mice on the variety of immunological researches. Lab Anim Res. 2017;33(2):119-23.

22. Tomayko MM, Reynolds CP. Determination of subcutaneous tumor size in athymic (nude) mice. Cancer Chemother Pharmacol. 1989;24(3):148-54.

23. Haase J, Misiak D, Bauer M, Pazaitis N, Braun J, Potschke R, et al. IGF2BP1 is the first positive marker for anaplastic thyroid

carcinoma diagnosis. Modern Pathol. 2021;34(1):32-41.

24. Jiang Z, Sun H, Yu J, Tian W, Song Y. Targeting CD47 for cancer immunotherapy. J Hematol Oncol. 2021;14(1):180.

25. Bishop JA, Sharma R, Westra WH. PAX8 immunostaining of anaplastic thyroid carcinoma: a reliable means of discerning thyroid origin for undifferentiated tumors of the head and neck. Hum Pathol. 2011;42(12):1873-7.

26. Lai WA, Hang JF, Liu CY, Bai YH, Liu ZY, Gu HY, et al. PAX8 expression in anaplastic thyroid carcinoma is less than those reported in early studies: a multi-institutional study of 182 cases using the monoclonal antibody MRQ-50. Virchows Arch. 2020;476(3):431-7.

27. Miettinen M, Franssila KO. Variable expression of keratins and nearly uniform lack of thyroid transcription factor 1 in thyroid anaplastic carcinoma. Hum Pathol. 2000;31(9):1139-45.

28. Lu L, Wang JR, Henderson YC, Bai S, Yang J, Hu M, et al. Anaplastic transformation in thyroid cancer revealed by single-cell transcriptomics. J Clin Invest. 2023;133(11).

29. Ferrari SM, Fallahi P, Galdiero MR, Ruffilli I, Elia G, Ragusa F, et al. Immune and Inflammatory Cells in Thyroid Cancer Microenvironment. Int J Mol Sci. 2019;20(18).

30. Chakraborty S, Carnazza M, Jarboe T, DeSouza N, Li XM,

Moscatello A, et al. Disruption of Cell-Cell Communication in Anaplastic Thyroid Cancer as an Immunotherapeutic Opportunity. Adv Exp Med Biol. 2021;1350:33-66.

31. Luo H, Xia X, Kim GD, Liu Y, Xue Z, Zhang L, et al. Characterizing dedifferentiation of thyroid cancer by integrated analysis. Sci Adv. 2021;7(31).

32. Zanello A, Bortolotti M, Maiello S, Bolognesi A, Polito L. Anti-PD-L1 immunoconjugates for cancer therapy: Are available antibodies good carriers for toxic payload delivering? Front Pharmacol. 2022;13:972046.

33. Choi Y, Shi Y, Haymaker CL, Naing A, Ciliberto G, Hajjar J. T-cell agonists in cancer immunotherapy. J Immunother Cancer. 2020;8(2).

34. Waldman AD, Fritz JM, Lenardo MJ. A guide to cancer immunotherapy: from T cell basic science to clinical practice. Nat Rev Immunol. 2020;20(11):651-68.

35. Michielin O, Lalani AK, Robert C, Sharma P, Peters S. Defining unique clinical hallmarks for immune checkpoint inhibitor-based therapies. J Immunother Cancer. 2022;10(1).

36. Kyi C, Postow MA. Immune checkpoint inhibitor combinations in solid tumors: opportunities and challenges. Immunotherapy. 2016;8(7):821-37.

37. Schadendorf D, Hodi FS, Robert C, Weber JS, Margolin K, Hamid O, et al. Pooled Analysis of Long-Term Survival Data From Phase II and Phase III Trials of Ipilimumab in Unresectable or Metastatic Melanoma. J Clin Oncol. 2015;33(17):1889-94.

38. Nucera C, Nehs MA, Mekel M, Zhang X, Hodin R, Lawler J, et al. A novel orthotopic mouse model of human anaplastic thyroid carcinoma. Thyroid. 2009;19(10):1077-84.

국문 초록

서론: 면역종양학에서 마우스 모델을 확보하는 것은 새로운 치료 대상을 식별하고 검증하는데 중요하다. C57BL/6 마우스는 동물의 면역체계 중 가장 특성화된 것 중 하나로, 면역종양학에서 새로운 발견을 위한 가장 효과적인 플랫폼을 제공한다. TBP3743(마우스 갑상선 역형성암) 세포를 B6129SF1 하이브리드 마우스에 사용하여 정위이식 모델이 구축되었으며, 이 모델은 C57BL/6 계통 마우스에 비해 종양 면역학 연구에 있어서 제한 된다. 본 연구는 C57BL/6 마우스에서 새로운 정위이식 ATC 모델을 구축하고, 해당 모델에서 종양 미세환경의 면역특성을 중심으로 연구를 진행하였다.

방법: Adapted TBP3743 세포는 C57BL/6 마우스에서 in vivo serial passaging을 통하여 만들어졌다. 그리고 다음과 같이 마우스 갑상선에 정위이식 하였다: original TBP3743 세포를 주입한 B6129SF1 마우스 (original/129), adapted TBP3743 세포를 주입한 B6129SF1 마우스 (adapted/129) 및 adapted TBP3743 세포를 주입한 C57BL/6 마우스 (adapted/B6).

결과: Adapted TBP3743 세포는 체외에서 세포 모양, 생존율, 이동/침습 능력은 original TBP3743 세포와 비교하였을 때 비슷하였다. Ki-67^+ 세포 분획은 original/129에 비해 adapted/129에서 더 높은 결과를 보였다. 정위이식 종양 RNA sequencing 데이터 분석을 통하여

adapted/129는 original/129에 비하여 더 강한 oncogenic properties를 보여주었다. 반면, adapted/B6에서 성장한 정위이식 종양은 adapted/129보다 크기가 작고 낮은 $Ki-67^+$ 세포 분획을 보였다. 그러나 adapted/B6와 adapted/129에서의 oncogenic properties는 유사했다. Immune-related pathways는 adapted/B6에서 adapted/129와 비교하여 풍부하게 발현되었다. 정위이식 종양의 유세포분석 결과, adapted/B6에서 세포독성 $CD8^+$ T세포와 monocytic-myeloid-derived suppressor 세포 분획이 모두 adapted/129보다 높았다. adapted/B6에서 추정된 $CD8^+$ 및 $CD4^+$ 세포 분획은 인간 ATC에서와 유사하지만 original/B6에서는 무시할 수 있었다.

결론: 위 연구를 통해 C57BL/6 마우스에서 역형성 갑상선 암의 새로운 정위이식 모델을 성공적으로 수립하였다. 기존의 B6129SF1 마우스 모델과 비교하면, 이 모델은 더 공격적인 종양특성과 강력한 면역반응을 나타낸다. 또한 이 모델은 종양의 미세환경을 더 깊이 연구하는데 활용되고, 새로운 항암제 개발을 위한 플랫폼으로서 작용할 것이다.

주요어: 갑상선 역형성암, 동계, 종양 미세환경, 면역 치료

학번:2017-36136